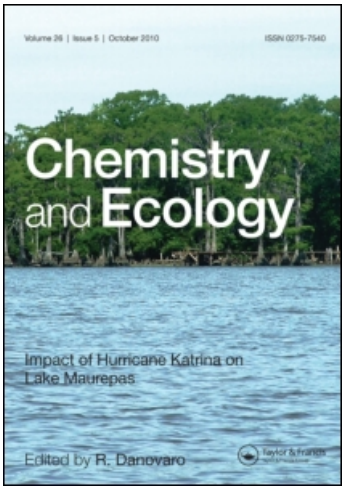

Chemistry and Ecology
Publication details, including instructions for authors and subscription information:
http://www.informaworld.com/smpp/title~content=t713455114

Heavy metals in top core sediments from the southern Campania shelf (Italy): Hints to define large-scale geochemical backgrounds

Mario Sprovieri[a]; Simone Sammartino[a]; Daniela Salvagio Manta[a]; Ennio Marsella[a]; Luciana Ferraro[a]
[a] Istituto per l'Ambiente Marino Costiero (IAMC), CNR, Calata Porta di Massa, Napoli, Italy

To cite this Article Sprovieri, Mario , Sammartino, Simone , Manta, Daniela Salvagio , Marsella, Ennio and Ferraro, Luciana(2006) 'Heavy metals in top core sediments from the southern Campania shelf (Italy): Hints to define large-scale geochemical backgrounds', Chemistry and Ecology, 22: 1, 65 — 91
To link to this Article: DOI: 10.1080/02757540500456716
URL: http://dx.doi.org/10.1080/02757540500456716

Chemistry and Ecology
Vol. 22, No. 1, February 2006, 65–91

Taylor & Francis
Taylor & Francis Group

Heavy metals in top core sediments from the southern Campania shelf (Italy): Hints to define large-scale geochemical backgrounds

MARIO SPROVIERI*, SIMONE SAMMARTINO, DANIELA SALVAGIO MANTA, ENNIO MARSELLA and LUCIANA FERRARO

Istituto per l'Ambiente Marino Costiero (IAMC), CNR, Calata Porta di Massa, Interno Porto di Napoli, 80100 Napoli, Italy

(Received 5 September 2005; in final form 26 October 2005)

The results of a geochemical survey carried out on the southern Campania shelf (southern Italy) are illustrated, offering a tempting opportunity to discuss the statement and definition of regional geochemical backgrounds for selected heavy metals. A total of 104 top core sediments, collected on average 1.5 km from one another and covering a shelf area of about 1300 km^2, were analysed for grain size, organic carbon content (OC), and heavy-metal (As, Al, Fe, Cd, V, Cr, Zn, Cu, Ni, Hg, and Pb) concentrations. The characteristics of the area, scarcely influenced by industrial activities, and the extensive data set, make this study suitable for an appropriate multivariate and spatial geostatistical methodologies used for i) a reliable definition of large-scale marine sediments' geochemical backgrounds and ii) an accurate discrimination of different geological controls on trace-element distribution patterns. Enrichment factors estimated with respect to both the average shale composition and the weighted average metal concentrations measured in inland soils rule out significant anthropogenic inputs. A spatial-geostatistics approach (kriging of spatial component based on an accurate implementation of variographic surveying) was applied, and this is proposed as an appropriate quantitative methodology to define the geochemical backgrounds for the different heavy metals. Two nested spatial structures were identified for some of the heavy metals, thus allowing clear identification of local and regional geochemical controls related to the different spatial variability of grain size.

Keywords: Heavy metals; Geostatistics; Variography; Geochemical backgrounds; Marine sediments

1. Introduction

The definition of geochemical background maps for selected trace elements is fundamental for the assessment of environmental changes induced by the anthropogenic impact. This led many countries to compile multi-element regional geochemical atlases (*e.g.* [1–3]). Regional surveys have already been carried out in some countries (*e.g.* [4–21]), and with increased national and international funding they can be extended to cover the rest of the land surface of the globe. Establishment of such an integrated global database is under the auspices of

*Corresponding author. Email: mario.sprovieri@iamc.cnr.it

Chemistry and Ecology
ISSN 0275-7540 print/ISSN 1029-0370 online © 2006 Taylor & Francis
http://www.tandf.co.uk/journals
DOI: 10.1080/02757540500456716

the International Union of Geological Surveys (IUGS) and the International Association of Geochemistry and Cosmochemistry (IAGC). In particular, the Global Geochemical Baseline Programme of the IUGS/IAGC is described with particular reference to the standardization of geochemical survey methods worldwide and the provision of a Global Reference Network (GRN) against which new and available national and regional geochemical datasets will be levelled. Contemporary, multivariate stationary geostatistical methodologies have been implemented to appropriately assess the background levels for different trace elements and define their sources and sinks in relation to regional and local basic geology and sedimentary features (*e.g.* [15, 22–32]).

Geochemical backgrounds provide a means of defining the natural spatial variations in the geochemistry of the earth's surface materials for the guidance of policy-makers concerned with environmental issues. Appropriate definitions of geochemical backgrounds are needed for environmental legislation and political decision-making, especially in the assessment of contaminated areas and definition of concentration levels that put human health and the ecosystem at risk. Moreover, the definition of geochemical backgrounds for toxic heavy metals is becoming increasingly necessary for coastal and shelf marine sediments where several industrial wastes and discharges and commercial ports are located. In many areas of Italy, natural concentrations of several heavy metals exceed the defined limit values designated for contaminated soils generally because of anthropogenic pollution but at times due to a geological context characterized by natural high levels of different heavy metals. Thus, it would seem reasonable that for political decision-making, separate local and regional backgrounds should be determined with separate guidelines for constituents determined by different analytical procedures.

However, although the term 'geochemical background' appears in the international geochemical mapping programmes of both IGCP 259 and 360 [10], its definition has already become vague. Generally, the 'geochemical baseline' of an element is considered as its natural variation in concentration in the environment under study with direct control of regional and/or basic geology. This definition is undermined by an appropriate definition of the factors (collection methods and measurement techniques) that strongly influence the concentration values of the different analytics. While an international standardization of these primary parameters is pending, it is necessary to describe each parameter for every geochemical background definition of selected areas.

In this study, we propose a geostatistical approach focused on the assessment of the geochemical background for selected heavy metals in marine sedimentary environments characterized by limited anthropogenic inputs. The application of a proper variography together with kriging estimates is proposed to directly analyse dualistic behaviours of different trace elements and accurately infer their spatial structural variability related to different control mechanisms. Such an approach is focused on discrimination of different spatial scales in the heavy-metal background levels and to emphasize different lithologic and geologic controls on the metal distribution patterns ([33]). Application of variographic analysis and geostatistical estimations, implemented in a *quasi-stationary* multivariate framework, are proposed as appropriate and synthetic interpretation tools of the geochemical dataset and represent a powerful numerical approach to appropriately assess trace elements natural backgrounds.

As a case study, the Campania shelf area was investigated within the bathymetry of 200 m. It represents an outstanding natural laboratory to investigate different contributions of heavy metals to the coastal marine system and to test the stationary and non-stationary geostatistical methodologies that can be used for the definition of the geochemical baselines. The complex lithogenic system, typical of a volcanogenic area and characterizing most of the eastern Tyrrhenian region, renders the southern Campania shelf area one of the most complex environmental systems to define and identify geochemical baselines and geochemical anomalies.

2. Materials and methods

2.1 *Geological context*

The shelf of the Eastern Tyrrhenian Sea margin lies in a tectonic transition zone between the uplifting Appennine chain to the east (on land) and the subsiding Tyrrhenian Basin [34–36]. The study area encompasses the shelf between the Gulf of Salerno and the Gulf of Policastro. Seaward of the study area lies the youngest part of the Tyrrhenian Bathyal Plain, an area where subsidence is inferred to be about 1 mm/yr during post-early Pleistocene [36]. Three different physographic settings exist in this region: Salerno Gulf, Cilento Promontory, and Policastro Gulf.

The Gulf of Salerno and the Sele River Plain on land constitute a structural depression (perytyrrhenian basin) trending WSW–ENE, bounded by NW–SE normal faults with an offset of about 3000 m [37, 38] of the Mesozoic and Cenozoic Apenninic Units and filled by Plio-Quaternary sediments 100 m thick [39–41]. The northern part of the Salerno Gulf is characterized by a steep to very steep slope dipping more than 10°, a shelf-break at 100–120 m water depth, and a narrow shelf (1 km to a few kilometres wide). The area of the wide shelf (max 30 km), in the southern part of the Salerno Gulf, north of Cape Licosa, has a deeper shelf-break (180 to more than 200 m water depth). A change in bathymetric gradient at 120 m depth marks the transition to the outer shelf. The sea-floor surface is steeper ($>1°$) landward of the transition and becomes gentler ($<0.5°$) on the outer shelf [42]. Off Cape Palinuro, the shelf presents a width of about 23 km with a shelf-break located at 250 m of water depth. East and south of Cape Licosa, the shelf narrows, and the shelf-break is located at a water depth of 130–150 m [43].

The Gulf of Policastro is characterized by a narrow shelf (2–5 km wide) and a very steep upper slope ($>10°$). A large number of gullies, at places indenting the shelf-break, extensively dissect the upper slope. Close to the shelf-break, wide slump scarps are commonly formed, while slump folds occur on the slope. These indicate that downslope mass transfer has involved large volumes of sediments [44].

2.2 *Sampling method*

Samples were collected during the GMS 03_01 oceanic cruise (aboard the O/V *Urania* vessel) in November 2003. The location map of the collected samples is reported in figure 1. Surficial sediments were collected by a Van Veen grab, and immediately described in terms of visible features and grain size. Three sub-samples were collected from the surficial 2 cm of sediment, placed into pre-cleaned Ziploc plastic bags for trace-metal analysis and stored at $-18°C$ on board within an hour of collection. Special attention was paid to avoid problems of contamination.

2.3 *Analytical methods*

2.3.1 Grain size. The mean grain size of sediments was estimated by visual comparison according to the classic Udden–Wentworth scale for clastic sediments ([45]) and calibrated by laboratory analysis of 10 samples. In this case, grain sizes were determined gravimetrically after wet sieving and after a pretreatment with H_2O_2. Sediment samples were classified as fine particles (silt + clay) (average $\phi < 0.06$ mm), fine sand ($0.063 < \phi < 0.250$ mm), medium sand ($0.250 < \phi < 0.500$ mm), coarse sand ($0.500 < \phi < 1.000$ mm), and very coarse sand ($\phi > 1.000$ mm) using five numerical codes (from I to IV) as shown in table 1.

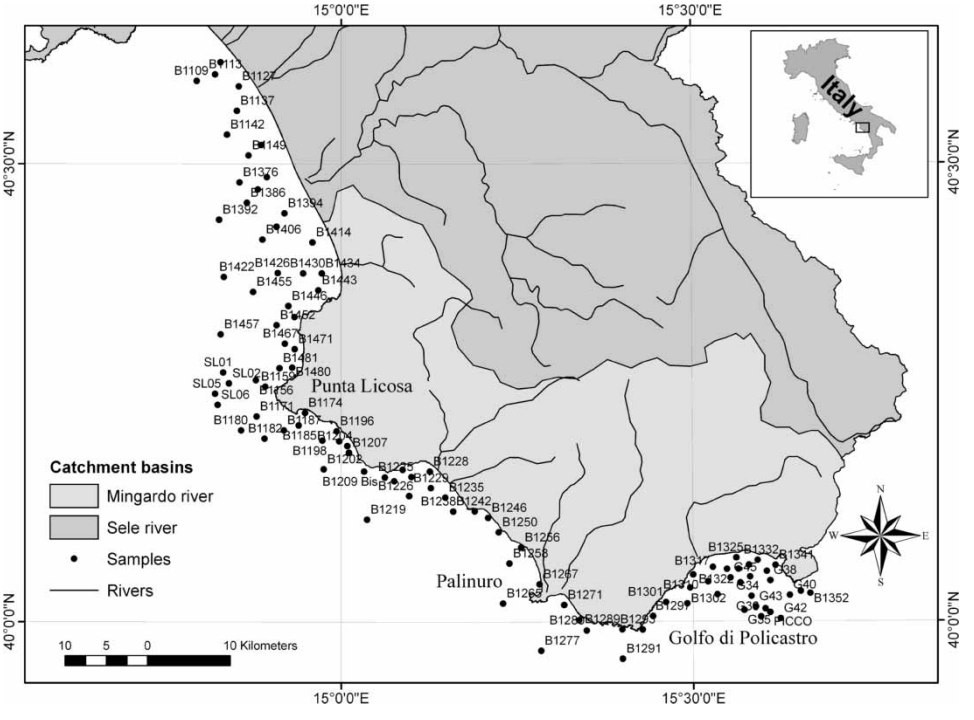

Figure 1. Map of the southern Campania shelf area and sampling sites. The two principal catchment basins of Southern Campania were reported in a previous study [37].

Table 1. Grain sizes of 10 selected samples used to test the Udden–Wentworth visual determination of granulometry of studied sediments.

Sample	Sand (%)	Silt (%)	Clay (%)	Grain size (classes)
B1202	5.12	57.2	14.7	I
B1238	11.1	67.6	21.3	I
B1340	22.3	63.2	14.5	I
B1271	48.7	45.0	6.3	II
B1414	45.2	46.2	8.6	II
B1289	60.6	35.1	4.3	III
SL01	64.1	32.3	3.6	III
SL05	68.3	28.9	2.8	III
B1348	83.2	14.3	2.5	IV
B1450	86.8	11.7	1.5	IV

2.3.2 Mineralogy. Sediments mineralogy was investigated by powder X-ray diffraction (XRD, Philips PW1729 apparatus) using CuKα radiation filtered by Ni. The relative proportions of minerals were determined according to methods and data of previous studies [46, 47].

2.3.3 Heavy metals. 'Pseudo-total metal contents' were obtained by digesting samples previously air-dried and sieved through a 2-mm sieve, with aqua regia in Teflon bombs using a microwave oven (CEM Mars X equipment) at a controlled pressure and temperature (110 psi

(758 kPa), 175°C, 100% power for 1 h). The suspension was filtered through 0.45 mm GF/F glass microfibre filters (Whatman). The term 'pseudo-total' is accounted for by the aqua regia digestion which does not completely destroy silicates. This method is widely used in environmental geochemistry studies and recommended by the National Government regulation. Aluminium, Fe, Cr, Cu, Ni, V, Zn, Pb, Cd, and As were measured with an inductively coupled plasma atomic emission spectrophotometer (ICP-AES) using a Varian Vista MPX. Mercury was determined by ICP-AES exciting the analyte to a form volatile hydride in the Hydrides Generation reactor VGA 76P, according to a previously reported method [48]. All calibration standards were prepared in the same acid matrix used for the sediment samples. Caution was used in preparing and analysing samples to minimize contamination from air, glassware, and reagents, all of which were of Suprapur quality. Replicated measures of international reference materials (PACS2), reagent blanks, and duplicated soil samples (about 20% of the total number of samples randomly selected from the set) were used to assess contamination and precision. The analytical precision, measured as relative standard deviation, was routinely between 5 and 6%, and never higher than 10%. All results were calculated with respect to dry weight.

2.3.4 Total organic carbon (OC). Total organic carbon was determined using a Thermo-Electron Flash EA 1112 elemental analyser on freeze-dried powdered samples. The carbonate fraction was eliminated through HCl treatment in silver capsules.

2.4 *Geostatistical methods*

Spatial georeferenced data have been processed with the ISATIS geostatistical software package. This allows complete Exploratory Statistical Data Analysis (ESDA) and all variography and estimation techniques in stationary and non-stationary frameworks. The geodetic reference is the Universal Transverse Mercator (fuse 33) projected on DATUM WGS 1984. All the information has been managed in a GIS georeferenced environment, using the ArcGis 9.0 software package.

3. Results

3.1 *Sediment grain size*

Most of the samples (>40%) are fine (table 2). They are mainly distributed in the deepest areas (out of the coastal domain) and in the Golfo di Policastro. Fine sands (about 38%) are widely spread along the coast, mainly in the northern part of the study area and close to Punta Licosa. The remaining medium, coarse, and very coarse sandy sediments are located off Punta Licosa and in the southern area, around Capo Palinuro.

3.2 *Mineralogy*

A group of 10 samples, representative of the different lithologies and grain size classes, were analysed by XRD for mineralogical composition. Samples are dominated (*c*. 60%) by aluminosilicates minerals (clay minerals and feldspars) and quartz (average 35%). The carbonate contents range from 10 to 15%.

Table 2. Heavy metals, OC, and grain-size data along with basic statistical parameters.

Sample	Easting (m)	Northing (m)	Al (mg kg^{-1})	Fe (mg kg^{-1})	Cr (mg kg^{-1})	Cu (mg kg^{-1})	Ni (mg kg^{-1})	V (mg kg^{-1})	Zn (mg kg^{-1})	Pb (mg kg^{-1})	Hg (mg kg^{-1})	Cd (mg kg^{-1})	As (mg kg^{-1})	OC (%)	Grain size (classes)
B1107	485 413.67	4 495 639.84	15 103.96	19 979.420	18.63	7.03	12.78	78.59	61.98	11.57	0.010	0.160	27.44	0.19	II
B1113	484 735.41	4 494 164.53	34 934.77	30 005.970	39.68	22.56	22.21	65.07	77.52	23.56	0.040	0.360	15.97	1.11	II
B1127	487 619.80	4 492 709.46	24 628.88	25 137.840	28.09	11.19	17.88	49.51	58.39	8.61	0.020	0.110	13.23	1.68	II
B1137	487 398.44	4 489 734.26	38 122.80	33 233.520	46.60	17.04	25.24	69.26	73.02	15.01	0.060	0.020	18.23	0.27	I
B1142	486 185.79	4 486 856.00	50 780.05	38 062.880	54.18	24.27	27.38	84.51	80.65	26.15	0.030	0.260	20.75	0.53	I
B1149	488 803.40	4 484 334.90	61 618.73	47 943.150	54.05	19.84	26.98	84.45	81.10	27.98	0.040	2.000	19.31	1.75	II
B1156	489 696.63	4 457 102.90	20 184.10	18 734.780	16.74	7.29	7.98	44.34	26.74	13.86	0.020	0.050	38.27	0.27	III
B1159	490 818.29	4 456 310.71	12 103.26	18 882.770	6.57	3.57	3.34	33.95	17.98	7.05	0.010	0.170	24.17	0.03	III
B1171	489 774.33	4 452 708.67	19 863.15	16 803.850	18.52	10.95	9.22	36.83	29.10	14.73	0.130	0.090	22.97	0.43	II
B1174	495 648.92	4 453 128.69	11 466.25	15 375.070	8.39	3.08	5.41	38.30	29.87	5.66	0.010	0.050	11.35	0.54	II
B1180	487 904.14	4 451 023.60	77 315.19	55 496.450	66.38	37.10	38.37	105.41	116.40	45.32	0.170	0.230	36.74	0.78	I
B1182	490 743.28	4 450 028.13	77 946.72	48 387.120	65.19	30.25	33.01	102.89	95.95	40.07	0.050	0.180	29.31	0.67	I
B1185	494 876.00	4 451 624.78	14 604.05	12 023.220	12.89	5.93	5.36	30.07	27.67	10.77	0.010	0.080	14.57	0.06	II
B1187	493 083.19	4 451 031.10	7 576.65	15 980.650	8.76	4.09	4.53	40.66	21.81	13.03	0.020	0.110	50.77	1.30	IV
B1196	499 473.68	4 450 908.13	7 455.50	16 474.580	26.36	13.79	15.15	50.22	53.28	18.09	0.040	0.090	22.86	0.03	II
B1198	497 732.90	4 449 775.40	26 889.73	26 958.460	30.59	16.06	17.44	57.45	61.47	21.52	0.030	0.160	26.65	0.93	I
B1201	499 785.98	4 449 694.66	17 805.06	14 121.940	9.19	3.29	6.13	26.15	25.13	4.73		0.040	20.34	1.63	II
B1202	497 904.69	4 446 294.83	53 192.18	44 280.330	57.20	36.41	38.24	88.68	110.35	42.28	0.120	0.240	30.51	0.70	I
B1204	500 774.51	4 449 122.54	9 518.35	12 176.130	8.77	3.38	6.56	23.81	28.76	4.18	0.020	0.060	15.27	12.32	II
B1207	500 974.52	4 448 307.50	7 399.38	10 559.770	7.31	2.92	5.75	19.91	27.19	3.63	0.010	0.030	17.56	1.13	II
B1209 Bis	502 797.04	4 446 034.96	8 713.12	13 355.700	8.08	3.71	6.32	29.33	24.71	8.02	0.010	0.060	23.92	0.35	IV
B1216	505 329.10	4 445 309.38	8 172.63	15 447.750	9.11	4.24	6.88	34.15	31.12	9.61	0.010	0.170	30.90	0.38	IV
B1219	503 172.26	4 440 189.91	42 862.50	36 998.520	50.50	24.72	27.13	78.04	79.39	25.54	0.040	0.210	20.64	1.55	I
B1221	506 446.77	4 444 853.22	35 431.94	29 052.500	28.40	12.63	17.96	44.34	61.86	11.39	0.040	0.010	17.03	0.28	II
B1224	507 468.00	4 446 238.00	14 938.70	18 589.900	16.55	8.41	12.93	28.43	56.14	5.68	0.290	0.020	13.24	1.65	II
B1225	508 541.00	4 445 357.00	33 928.00	25 447.100	29.44	11.42	16.43	48.14	53.75	12.27	0.020	0.040	12.52	0.19	II
B1226	508 269.00	4 443 051.00	52 476.80	38 447.600	53.84	27.65	29.14	83.52	90.46	28.22	0.060	0.180	21.78	1.37	I
B1228	510 769.00	4 446 025.00	23 267.50	22 325.800	24.53	10.64	17.20	41.22	63.60	8.63	0.210	0.060	13.94	0.09	I
B1228 Bis	510 786.00	4 446 007.00	19 664.10	21 502.400	21.20	9.43	15.86	35.81	56.23	6.98	0.020	0.090	12.78		II
B1229	510 884.00	4 444 018.00	16 682.90	23 053.700	22.37	16.52	18.73	34.43	62.48	10.65	0.030	0.080	11.62	2.02	II

B1235	512 648.00	4 442 869.00			31.31	13.70	20.59	48.65	61.38	12.72	0.040	0.090	15.74	0.24	II
B1238	513 595.00	4 441 176.00	71 861.10	59 623.600	56.00	32.48	34.30	77.13	103.60	22.73	0.130	0.080	20.94	0.86	I
B1242	516 209.00	4 441 205.00	12 583.00	17 151.400	12.49	6.64	13.71	25.00	65.08	11.77	0.010	0.140	12.97		IV
B1246	517 828.00	4 440 413.00	16 024.80	21 846.000	16.22	8.55	13.50	30.02	43.86	7.37	0.010	0.020	17.03	0.29	II
B1250	519 108.00	4 438 660.00	2 721.88	11 014.700	5.44	3.04	6.55	12.04	20.36	3.96	0.010	0.010	8.83	0.23	IV
B1256	521 836.00	4 436 817.00	7 045.33	12 476.700	8.37	3.94	7.28	13.94	30.86	2.77	0.010	0.030	6.81	0.49	IV
B1258	520 420.00	4 434 875.00	76 995.00	58 032.000	52.85	28.49	31.64	75.26	87.49	21.64	0.150	0.070	20.03	0.14	I
B1265	519 633.00	4 430 028.00	69 956.00	50 717.600	73.44	38.92	45.44	101.39	116.32	30.28	0.200	0.100	28.71	0.60	I
B1267	524 058.00	4 432 375.00	3 480.53	8 363.890	7.41	2.89	6.12	13.25	19.65	2.83	0.010	0.040	12.93	0.62	IV
B1271	527 040.00	4 429 865.00	37 478.90	37 938.300	31.72	21.29	29.14	41.42	65.22	12.78	0.020	0.090	6.47	0.07	II
B1277	524 264.00	4 424 315.00	74 907.40	49 274.700	72.82	35.20	39.85	106.37	105.74	38.41	0.060	0.190	32.82	0.47	I
B1278	528 861.00	4 428 016.00	27 616.50	28 556.500	25.41	15.12	21.42	36.20	52.80	8.74	0.030	0.100	8.66	1.47	II
B1280	529 785.00	4 426 775.00	36 545.00	32 907.700	35.00	19.70	25.47	51.79	85.87	14.34	0.030	0.300	10.97	0.50	II
B1289	534 082.00	4 426 927.00	18 177.60	21 862.100	18.84	11.29	15.08	30.38	54.21	8.07	0.050	0.070	9.75	0.40	III
B1291	534 149.00	4 423 350.00	71 020.40	43 953.400	68.12	31.99	40.23	93.05	111.41	25.18	0.040	0.040	18.78	0.33	I
B1293	536 561.00	4 426 906.00	643.29	11 269.700	5.28	2.02	3.17	27.27	18.74	8.68	0.010	0.080	43.18	0.19	III
B1297	537 832.00	4 428 551.00	74 651.50	68 519.700	59.39	34.26	38.33	85.10	111.19	25.14	0.160	0.120	29.71		II
B1301	539 388.00	4 430 222.00	73 786.80	53 612.900	71.15	34.99	40.37	106.32	106.48	31.06	0.060	0.320	24.78	0.78	I
B1302	541 976.61	4 430 071.26	62 240.45	46 759.500	71.44	38.75	45.01	104.18	120.25	34.51	0.050	0.220	25.15	0.55	I
B1308	542 312.40	4 432 008.16	71 638.75	45 980.120	86.21	39.40	43.85	113.10	124.86	23.06	0.040	0.040	22.45		I
B1310	542 674.43	4 433 578.58	75 380.17	52 019.040	70.03	34.24	35.96	92.76	89.84	16.51	0.350	0.050	17.41	0.13	I
B1315	544 489.86	4 432 741.53	98 158.59	45 939.250	79.77	34.49	39.00	105.37	110.66	20.88	0.060	0.050	18.70	0.66	I
B1317	545 068.74	443 4509.73	54 419.38	47 711.320	66.57	32.29	38.76	84.69	95.49	16.55	0.050	0.060	15.91	0.64	I
B1322	546 767.74	4 434 262.69	60.37			28.60	32.70	87.81	90.56	22.41	0.060	0.340	16.73	0.48	I
B1325	547 892.00	4 435 651.72	44 804.33	40 346.770	50.82	19.67	31.15	75.93	82.62	13.56	0.020	0.160	19.67	1.33	II
B1330	549 416.12	4 434 768.55	61 645.28	42 682.680	63.03	27.86	30.71	93.63	86.82	23.63	0.040	0.030	23.84	0.65	I
B1332	550 481.97	4 435 355.95	71 669.41	67 427.920	50.80	17.27	31.13	73.23	85.39	13.47	0.020	0.150	22.77	0.35	II
B1337	551 438.37	4 429 483.94	57 417.41	45 501.920	64.79	31.73	39.32	90.54	98.51	23.87	0.060	0.040	26.62	1.54	I
B1340	551 586.93	4 434 037.70	57 386.02	42 144.350	59.59	30.56	32.87	82.81	90.95	19.66	0.150	0.020	20.87	3.15	I
B1341	552 642.74	4 434 760.06	40 696.28	34 715.080	42.82	17.38	28.14	60.17	73.84	10.30	0.030	0.100	16.71	0.56	II
B1348	555 710.82	4 431 626.34	36 297.89	28 062.310	40.79	20.53	23.53	61.77	59.77	16.38	0.290	0.100	18.12	0.87	I
B1352	556 858.25	4 431 355.95	8 048.20	8 346.700	8.51	2.74	3.55	29.64	15.56	7.39	0.010	0.110	20.70	0.26	IV
B1374	491 007.10	4 481 711.64	26 746.67	26 327.440	33.90	11.90	20.58	50.80	53.96	8.44	0.050	0.230	11.95	0.27	II
B1376	487 714.27	4 481 072.72	68 109.77	42 992.560	75.22	36.57	36.12	107.74	104.75	30.53	0.040	0.330	21.32	0.66	II
B1380	489 924.21	4 480 230.87	47 556.51	35 594.740	54.70	21.87	26.93	80.91	75.78	19.27	0.030	0.190	15.01	1.74	I

(continued)

Table 2. Continued.

Sample	Easting (m)	Northing (m)	Al (mg kg^{-1})	Fe (mg kg^{-1})	Cr (mg kg^{-1})	Cu (mg kg^{-1})	Ni (mg kg^{-1})	V (mg kg^{-1})	Zn (mg kg^{-1})	Pb (mg kg^{-1})	Hg (mg kg^{-1})	Cd (mg kg^{-1})	As (mg kg^{-1})	OC (%)	Grain size (classes)
B1386	488 609.35	4 478 600.31	77 446.85	52 698.210	63.46	29.47	29.78	92.21	84.82	25.53	0.100	0.220	16.95	1.48	I
B1392	485 231.00	4 476 543.78	85 278.57	45 229.650	101.76	46.44	45.17	151.45	124.48	46.29	0.080	0.350	24.37	0.50	I
B1394	493 141.71	4 477 318.22	24 063.46	24 090.640	28.73	10.80	18.05	46.65	48.55	9.31	0.010	0.170	10.31	0.10	II
B1400	492 189.73	4 475 691.19	45 713.29	41 711.200	40.30	14.65	23.57	58.49	56.92	11.05	0.020	0.090	12.44	0.17	II
B1406	490 481.78	4 474 136.42	72 127.80	52 217.430	55.55	23.51	27.08	83.83	83.97	25.19	0.030	0.320	19.16	0.82	I
B1414	496 540.72	4 473 790.13	27 001.50	28 354.310	41.92	13.93	23.11	66.36	64.11	11.52	0.030	0.170	15.28	0.24	II
B1422	485 801.92	4 469 611.81	76 884.42	47 202.550	88.59	42.34	41.16	130.88	117.15	42.35	0.130	0.270	30.11	0.59	I
B1426	492 338.12	4 470 075.02	67 805.58	42 602.710	53.61	18.42	33.09	78.28	90.52	14.30	0.050	0.140	24.21	1.11	II
B1430	495 415.41	4 470 032.21	310 83.35	28 386.200	37.82	13.32	20.62	55.50	62.57	10.11	0.020	0.040	14.71	0.20	II
B1434	497 685.38	4 470 031.53			29.74	11.87	16.46	49.68	60.37	8.70	0.040	0.730	12.99	0.35	II
B1443	497 252.65	4 467 987.06	20 521.16	19 664.870	24.00	8.89	14.72	37.14	48.39	7.05	0.030	0.040	9.66	1.69	II
B1446	493 626.59	4 466 098.50	62 757.11	43 131.870	55.02	22.03	26.78	78.62	73.93	19.29	0.040	0.050	19.55	1.31	I
B1450	494 359.13	4 464 748.88	12 182.10	14 616.050	12.12	5.79	8.38	39.75	31.78	10.01	0.030	0.190	22.38	0.23	IV
B1452	492 185.25	4 463 764.66	46 042.27	30 852.340	44.21	19.21	22.23	72.12	67.62	22.65	0.020	0.140	15.86	1.39	II
B1455	489 352.41	4 467 806.67	77 178.89	53 674.240	68.44	33.20	34.40	101.69	105.01	32.51	0.060	0.250	23.72	0.78	I
B1457	485 431.05	4 462 645.10	69 164.09	44 667.240	72.47	31.71	36.16	103.35	99.47	32.17	0.100	0.010	29.41	0.41	I
B1467	493 185.60	4 461 524.50	29 383.82	27 021.940	34.12	15.51	20.63	57.66	63.31	17.96	0.030	0.050	21.64	0.66	I
B1471	494 393.09	4 460 857.90	4 996.95	10 934.140	7.25	1.72	4.26	21.96	23.62	2.75	0.010	0.010	29.39	0.07	III
B1480	494 081.50	4 458 616.30	4 962.91	11 154.580	4.60	1.15	2.81	27.40	13.38	2.75	0.010	0.040	34.27	0.60	IV
B1481	492 555.20	4 458 546.70			21.38	10.06	12.38	63.91	56.32	15.54		0.080	35.29		III
BX-1364	490 340.66	4 485 600.86	31 200.00	30 164.850	38.77	12.43	23.09	55.53	60.85	9.47	0.020	0.010	13.36	0.83	III
CUMULI	545 610.96	4 431 200.14	69 987.41	49 050.890	66.46	33.63	38.99	94.51	93.61	18.41	0.140	0.060	18.32	0.46	I

G30	548 169.14	4 434 292.24	61 501.44	45 233.640	67.31	32.32	38.14	93.16	101.68	22.87	0.050	0.030	22.31	0.53	I
G31	548 385.96	4 432 630.52	66 621.59	44 618.330	62.08	32.11	37.67	95.43	107.49	25.76	0.050	0.470	18.15	0.40	I
G32	549 563.84	4 433 355.75	78 429.54	45 494.570	74.58	31.69	36.50	111.71	99.25	33.47	0.060	0.160	33.58	0.43	II
G34	549 745.68	4 431 004.69	50 146.09	41 045.330	54.38	28.14	35.32	76.77	82.06	22.43	0.090	0.050	25.21	0.41	I
G35	548 874.02	4 429 291.19	68 592.92	55 284.370	58.04	33.78	41.75	78.63	89.70	27.25	0.110	0.070	19.09	1.35	I
G36	550 911.37	4 428 511.02	75 228.63	53 716.290	75.31	37.44	45.82	105.76	106.28	37.50	0.080	0.280	35.06	0.39	II
G38	552 018.62	4 432 902.11			49.60	21.20	29.28	72.79	75.66	16.98	0.030	0.300	15.08		II
G40	554 397.04	4 431 136.27	60 826.19	39 800.450	62.97	27.70	36.21	86.81	83.49	21.81	0.060	0.070	20.52	0.97	I
G42	553 278.96	4 428 298.37	49 097.92	46 614.850	56.51	35.98	43.94	76.71	107.09	29.07	0.170	0.210	20.38	0.51	I
G43	550 284.76	4 429 715.84	46 047.70	43 947.970	52.11	31.66	38.80	73.48	84.67	24.78	0.170	0.160	27.73	1.70	I
G45	547 198.59	4 433 228.02	62 834.97	51 043.220	61.38	31.82	36.19	90.81	99.34	29.83	0.070	0.160	30.88		I
PICCO	552 011.70	4 429 037.91	48 876.92	35 550.900	46.30	22.97	30.15	67.37	81.19	23.29	0.050	0.210	12.14	0.31	V
SL01	485 720.50	4 458 046.80	33 719.61	36 597.060	21.10	13.96	19.42	83.60	51.51	17.79	0.030	0.480	24.70	0.35	III
SL02	486 438.40	4 456 723.30	5 335.93	13 828.770	5.79	4.16	5.98	35.77	44.53	8.69	0.020	0.220	28.48	0.13	V
SL05	484 735.80	4 455 467.20	7 614.32	7 941.690	4.49	2.34	2.49	15.72	12.03	9.55	0.010	0.140	17.57	1.87	III
SL06	485 069.65	4 454 109.98	497.00	4 540.160	4.46	3.25	3.09	14.99	11.99	7.78	0.130	0.010	24.22	0.25	IV
Min.			497.00	4 540.000	4.46	1.15	2.49	12.04	11.99	2.75	0.002	0.009	6.47	0.03	
Max.			98 159.00	68 520.000	101.76	46.44	45.82	151.45	124.86	46.29	0.350	2.000	50.77	12.32	
Mean			41 389.00	33 369.000	41.16	19.60	24.05	65.24	69.81	18.00	0.060	0.150	20.85	0.82	
Median			40 696.00	35 551.000	42.37	18.81	25.36	68.31	73.43	16.44	0.040	0.100	20.18	0.53	
Interquatile range			51 123.00	26 619.000	42.14	22.54	22.44	49.59	40.12	15.57	0.040	0.140	9.57	0.70	
S.D.			25 871.00	15 415.000	24.20	12.12	12.81	29.85	30.43	10.42	0.060	0.220	7.92	1.30	
Skewness			0.07	0.003	0.06	0.13	−0.13	0.13	−0.22	0.67	2.190	6.150	0.85	7.12	
Kurtosis			1.70	1.980	1.94	1.76	1.80	2.32	2.05	2.82	8.340	51.130	4.14	62.40	

3.3 *Heavy-metal contents and basic ESDA statistics*

The concentrations of heavy metals and organic carbon (OC), along with basic statistical parameters are shown in table 2. Among the metals, V has the highest values (12–151 mg kg^{-1}), followed by Zn (11–124 mg kg^{-1}), Cr (4–101 mg kg^{-1}), Cu (1–46 mg kg^{-1}), Ni (2–46 mg kg^{-1}), Pb (1–46 mg kg^{-1}), As (6–51 mg kg^{-1}), Cd (0.009–0.4 mg kg^{-1}), and Hg (0.002–0.3 mg kg^{-1}). Aluminium and Fe show average concentrations of 9.8 and 6.8%, respectively.

Aluminium, Fe, and most trace metals (Cr, Cu, Ni, V, and Zn) show quite a normal distribution, except for Cr and V, which show a slight deflection for a binomial one (table 2). The kurtosis index generally indicates a wide dispersion of values, with some slight platicurtic behaviour. All these characteristics are typical of large spatial domains (*e.g.* [49]); in our case, samples were collected over a very large wrap, 20 km wide, and more than 100 km long. Mercury, Cd, and OC show a different general behaviour with a high skewed distribution and a few large values which could, in a first approximation, be considered as outliers. Only As and Pb show a log-normal distribution, even if their logarithmic transformation leads to only a slight increase in normality in their histograms.

Aluminium, Fe, Cr, Cu, Ni, V, Zn, and, to a lesser extent, Pb show a significant negative correlation (table 3) with grain size: the Pearson coefficients range from -0.6 to -0.8. The -0.6 value for the Pb/grain size correlation decreases to -0.44 for log-transformed Pb. Also, the log-transformed Cd and Hg values present a lower correlation degree with grain size when compared with the same relationships calculated with untransformed data. As expected, low heavy-metal concentrations are characteristics of a coarse sediment, whereas fine particles show higher values. The clear relationship between grain size and most of the element distribution suggests that the mean grain size distribution is a dominant driving factor for elemental composition of the studied coastal sediments. Only As, Cd, Hg, and OC show a scarce correlation with grain size, thus suggesting different driving factors for their spatial distribution patterns.

Iron, Cr, Ni, Cu, Zn, and V show a high positive correlation (averagely >0.7) with Al (table 3) and high negative correlation values with grain size, thus suggesting an important control of alumino-silicates minerals, which account for more than 50% of the mineralogy of the sediments, on the distribution patterns of these elements.

Scatter plots of As with most of the other trace metals (Al, Fe, Cu, Ni, Zn, V, and Pb) generally show a bimodal distribution (see figure 2 as an example) with two main groups of samples and two different linear trends: group A, composed of low concentration values of As

Table 3. Correlation matrix of the studied sedimentary and geochemical parameters.

	Al	Fe	Cr	Cu	Ni	V	Zn	Pb	Hg	Cd	As	OC	Grain size
Al	1.00	0.95	0.95	0.92	0.92	0.92	0.92	0.81	0.36	0.23	0.17	−0.07	−0.70
Fe	0.95	1.00	0.90	0.89	0.92	0.86	0.91	0.76	0.36	0.25	0.15	−0.08	−0.71
Cr	0.95	0.90	1.00	0.96	0.96	0.96	0.95	0.85	0.37	0.21	0.18	−0.07	−0.73
Cu	0.92	0.89	0.96	1.00	0.97	0.92	0.96	0.89	0.45	0.18	0.20	−0.06	−0.72
Ni	0.92	0.92	0.96	0.97	1.00	0.90	0.97	0.81	0.40	0.18	0.12	−0.07	−0.74
V	0.92	0.86	0.96	0.92	0.90	1.00	0.92	0.89	0.31	0.28	0.32	−0.09	−0.68
Zn	0.92	0.91	0.95	0.96	0.97	0.92	1.00	0.84	0.39	0.22	0.13	−0.06	−0.77
Pb	0.81	0.76	0.85	0.89	0.81	0.89	0.84	1.00	0.31	0.33	0.43	−0.08	−0.60
Hg	0.36	0.36	0.37	0.45	0.40	0.31	0.39	0.31	1.00	−0.05	0.08	−0.02	−0.38
Cd	0.23	0.25	0.21	0.18	0.18	0.28	0.22	0.33	−0.05	1.00	0.06	0.03	−0.14
As	0.17	0.15	0.18	0.20	0.12	0.32	0.13	0.43	0.08	0.06	1.00	−0.10	0.07
TOC	−0.07	−0.08	−0.07	−0.06	−0.07	−0.09	−0.06	−0.08	−0.02	0.03	−0.10	1.00	−0.09
Grain size	−0.70	−0.71	−0.73	−0.72	−0.74	−0.68	−0.77	−0.60	−0.38	−0.14	0.07	−0.09	1.00

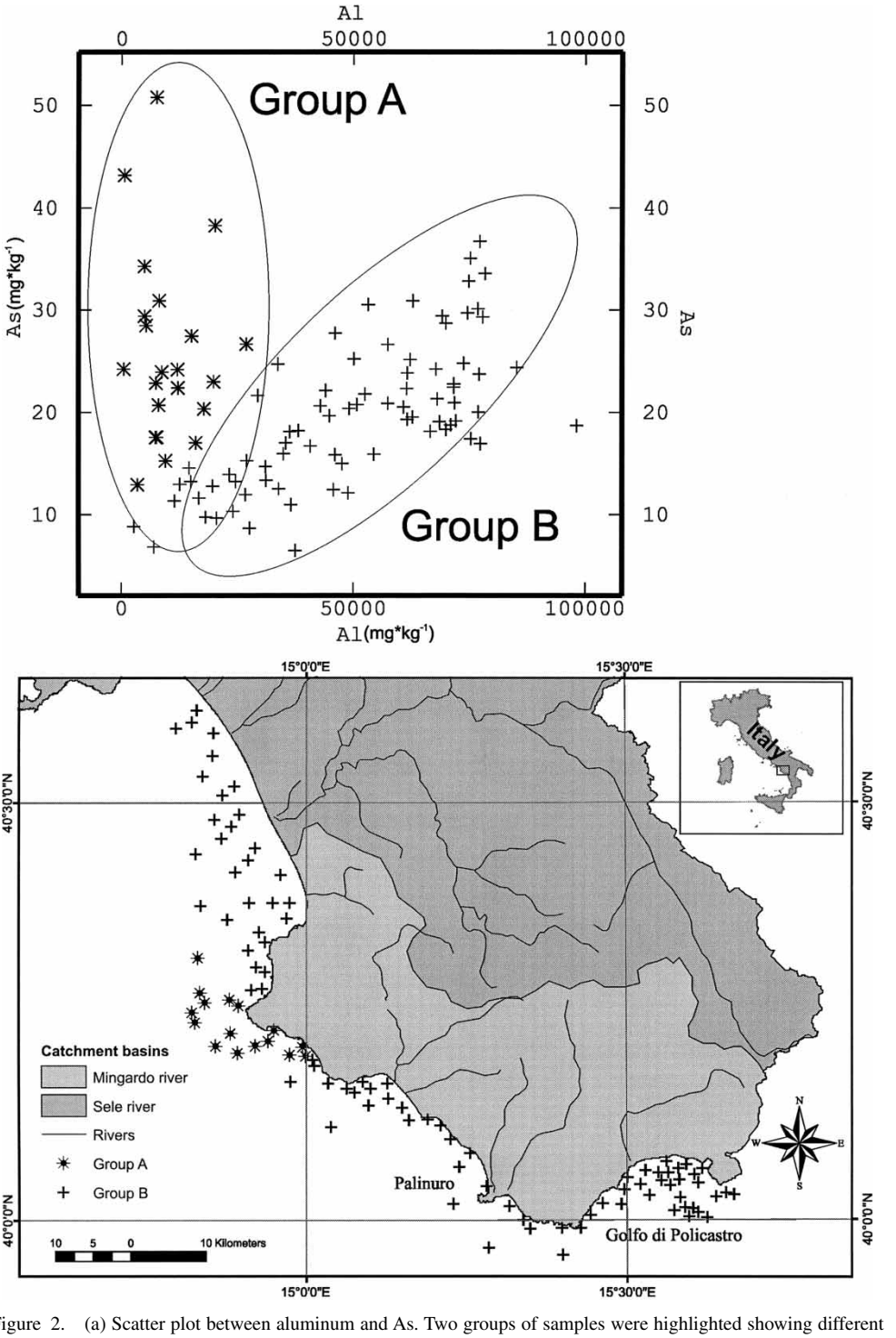

Figure 2. (a) Scatter plot between aluminum and As. Two groups of samples were highlighted showing different distribution patterns of the two elements. Samples of Group A are marked with asterisks and Group B with crosses on map (b).

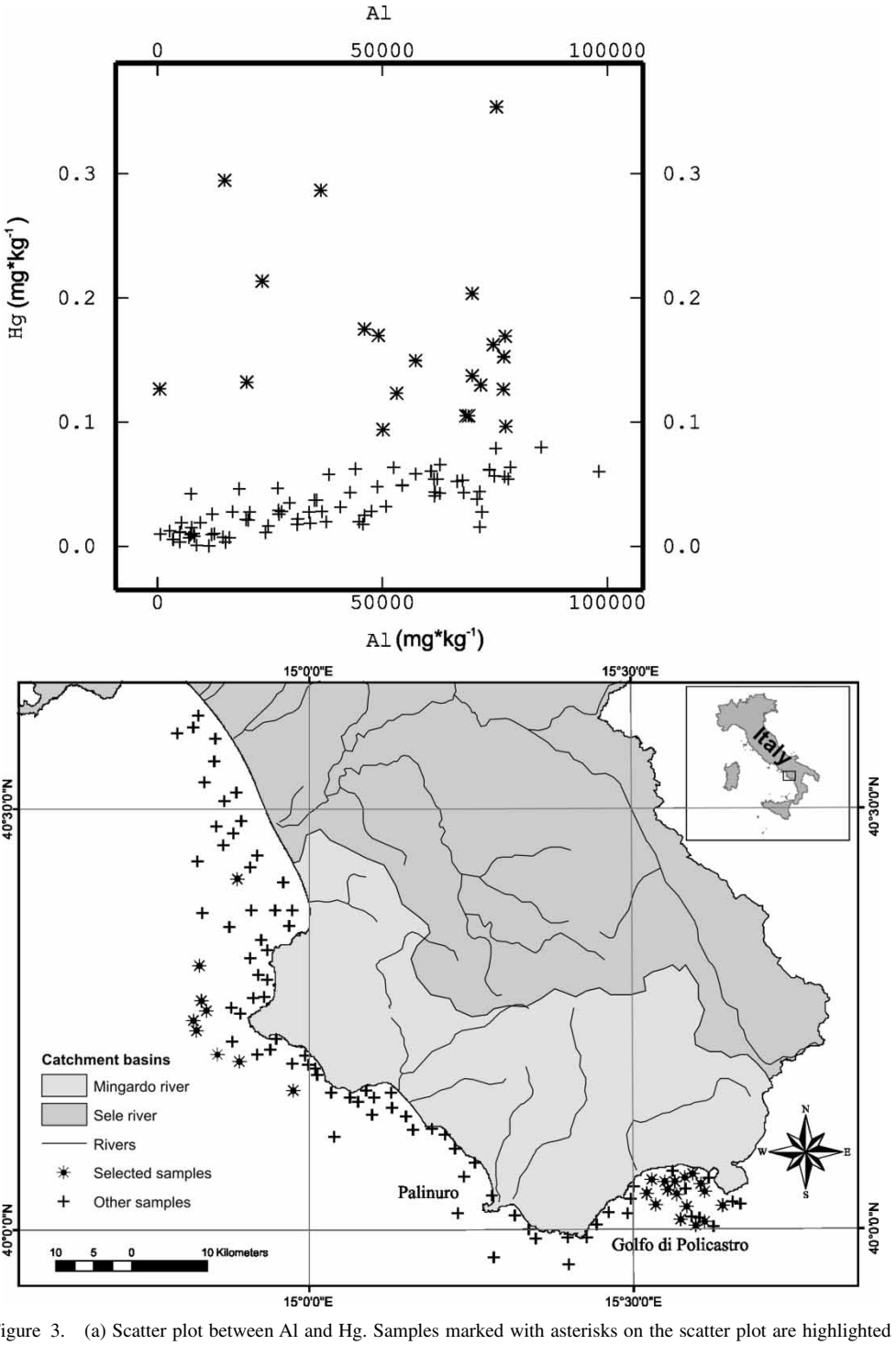

Figure 3. (a) Scatter plot between Al and Hg. Samples marked with asterisks on the scatter plot are highlighted with asterisks on map (b).

and a wide range of variability of other heavy metals; and group, B composed of co-varying As and other selected heavy metals. Group A is mainly concentrated around Punta Licosa, where grain size is generally characterized by sandy sediments, while group B is widely spread through the rest of the spatial domain. Mercury and Pb show a similar bimodal distribution of samples in the scatter plots among themselves and most other trace metals (figure 3), with one group of well-correlated samples and another group with scattered values in the plot. In this case, the poorly correlating group is widely distributed out of Punta Licosa and in the Golfo di Policastro zones. Cadmium and OC are generally poorly correlated with most of the other trace metals.

4. Discussion

4.1 *Enrichment factors*

In order to roughly discriminate sources of different heavy metals in the area, we calculated the enrichment factors (EFs) of the trace elements among the studied marine sediments and both the average shale values [50] and the weighted average concentrations previously reported [51] for the two hydrographic basin facing the studied marine shelf area. In particular, analytical procedures used for the analysis of our marine sediments and the continental samples of [51] are equivalent and allow a direct comparison of the two datasets.

Theoretically, the enrichment factor (EF), *i.e.* the ratio of an element to Al in marine sediments over that of the continental rocks, is capable of indicating the anthropogenic impacts because the concentrations of Al in weathering products and their parent materials are generally comparable (cf. [52] and references within).

The estimated EFs for the different heavy metals against values reported by [51] show that mean values are ∼1 (figure 4). A different picture can be observed for the enrichment factors calculated by comparing our marine sediments with the average lithospheric concentrations previously reported [50]. These results first exclude any kind of significant anthropic input on the distribution patterns of the different heavy metals in the studied area. Only As shows anomalously high EF values when compared with the average shale values attributable to

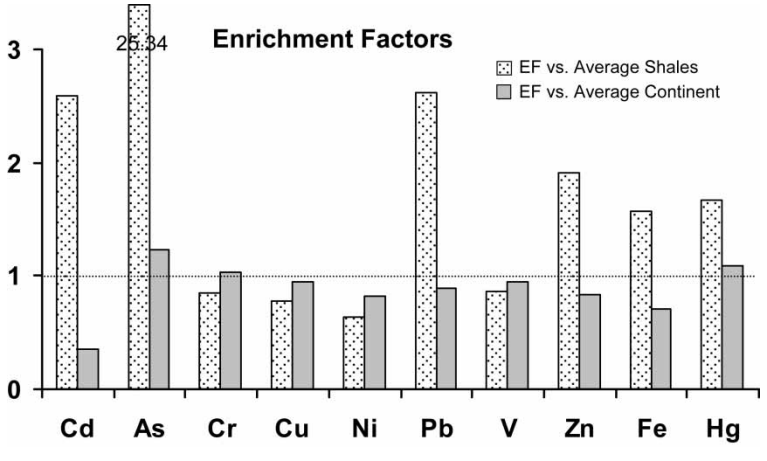

Figure 4. Enrichment factors for the different trace elements between the studied sediments against average shale values (dotted bars) [50] and the continental data (grey bars) [51] estimated for the facing catchment basins of southern Campania.

an important active hydrothermal circulation and related dissolution of As-bearing sulphides previously described [53–55] in the studied area. In fact, evidence from studies on reservoir fluids and epithermal ore deposits demonstrates that As is concentrated during hydrothermal processes [56–61]. In their study on the Phlegrean Field geothermal system, De Vivo *et al.* [53] give a 9–22 mg/l range for As content in the deep reservoir fluids, with pyrite and arsenopyrite being commonly recognized in the hydrothermal paragenesis.

4.2 *Quasi-stationary nested variography: a tool for the definition of natural geochemical backgrounds*

A variographic approach was used to quantitatively define the variability of the heavy metals at different spatial scales. Semivariance (half the squared difference between samples pairs) was calculated for each spatial class. Such classes are defined by dividing the entire spatial domain in regular lags and all the squared differences are averaged to extract one piece of information per class (semivariogram values). The result is a punctual distribution of values for spatial variance that in turn describes the spatial structure of the field. Usually adopted for estimation procedures, the experimental variogram needs to be modelled by a mathematical function in order to move from discrete distribution of variance to its continued theoretical model [62]. Such a model is called theoretical variogram, and its mathematical definition is used for a description of spatial structure applied in the kriging estimation process [63]. The main parameters of the model are:

(1) the nugget variance – the value of semivariance closely to zero lag distance;
(2) the range – the lag scale value that represents the spatial limit beyond which sample pairs are spatially uncorrelated; and
(3) the sill – the semivariance value reached at the range spatial scale (usually close to the global samples variance).

Generally, the approach is based on the *spatial stationary criteria* that assume the translation invariance of the mean value of the variable [64]. In particular, the second-order stationarity assumes that the mean value is constant through the entire spatial domain, and the variance of sample pairs does not depend on the spatial position but only on the lag distance. This condition is made less rigorous, assuming that the variable should not vary consistently at least inside a certain range of self-correlation among pairs. Such an approach allows us to lead a pure non-stationarity back to a stationary framework, making some assumption on the range of variability of the field and allowing the use of classical stationary variography. Such a situation is often called *quasi-stationarity*, generally studied assuming stationarity for a smaller scale within a reasonable self-correlation range [64]. In other words, we assume that non-stationary behaviour can be neglected, shrinking our application field to a smaller practical range within which the variable is effectively of a second order or intrinsic stationary (the so-called *local second-order/intrinsic stationarity)*. From a mathematical point of view, a quasi-stationary variable is characterized by a slightly variable mean varying very weakly through the entire spatial domain, so as to be considered invariant within certain ranges.

Experimental variogram computation parameters were defined, analysing the variogram map of the available pairs (the bi-dimensional polar map in which each cell represents the amount of pairs for a certain direction and a certain distance range), in which it is clear that a value of 1 km per lag is enough to obtain a reasonable quantity of pairs in each lag. Most of the omnidirectional experimental variograms of the studied trace metals, computed with a lag of 1 km and a total amount of 90 lags, show a reduced nugget variance at the smallest

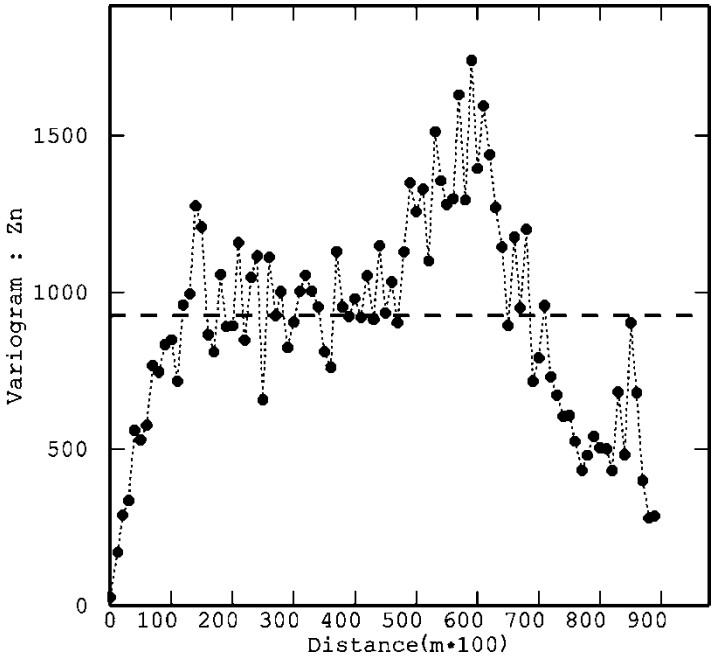

Figure 5. Experimental omnidirectional variogram for zinc. Experimental variogram is light dashed, while sample variance is bold dashed. See text for description of calculation parameters.

spatial scale, a well-structured bounding shape at a 20 km lag, with a well-defined range, and an unusual cuspid-shaped trend with a peak centred at a 60 km scale (figure 5).

If we take a look at the variogram cloud (figure 6a), and particularly at the pairs related to the 60 km scale, we can see how they are mainly driven by the high diversity between the zones of Policastro and Punta Licosa (figure 6b) characterized by a clear difference in grain-size distribution, finest at the Policastro area and generally sandy at Punta Licosa. Actually, the average differences between concentration values (expressed by the semi-variance values) reach their maximum at a scale of about 20 km. At this spatial scale, instead of varying slightly around the a priori variance and showing a spatial constant independence among pairs, they show an increasing semivariance score, induced by a direct comparison among samples belonging to the two above-mentioned zones. This type of behaviour is typical of a non-stationary framework, in which translation invariance of mean values is not ensured for all spatial scales. In this case, it is useful to turn to a *quasi-stationary* approach [64]. Variogram modelling is implemented within a stationary spatial scale; that is, all the spatial scales greater than that at which semivariance starts to behave asymptotically around the a priori *variance* (the range) are neglected. The theoretical model is considered constant beyond this limit [64]. In this way, it is possible to manage the problem within a classical stationary geostatistical framework. Moreover, it is useless to introduce weights from samples that are at a greater distance than the range limit; these are always statistically independent [49]. A complete and accurate knowledge of experimental variogram is very important to understand in detail the behaviour of the studied variables and their correlations with grain-size distribution, and its realistic modelling is essential for spatial estimation. Thus, neglecting the 'over-range' spatial scales and assuming the stationary behaviour of the different variables, we can implement a correct stationary estimation process, excluding this unusual long-range variability. Such an approach is reinforced by the assumption of an equal-pairs availability in all directions. The location map of the samples is extremely stretched along the shore, and consequently

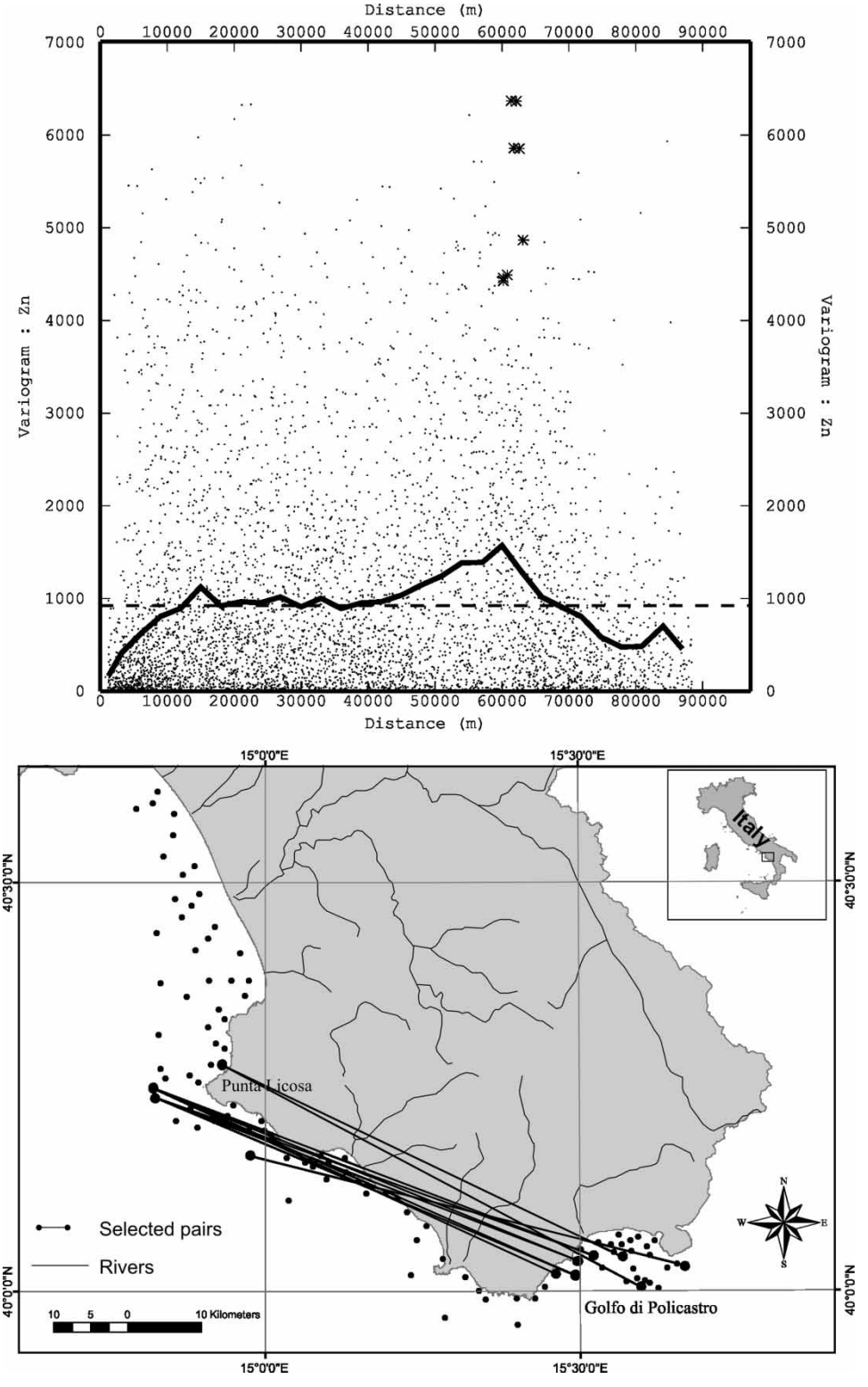

Figure 6. (a) Variogram cloud for zinc. (b) Map of the studied area with highlighted grey dots indicating the pairs of samples (centred on the Punta Licosa and Golfo di Policastro areas) that are the origin of the 60 km variability peak.

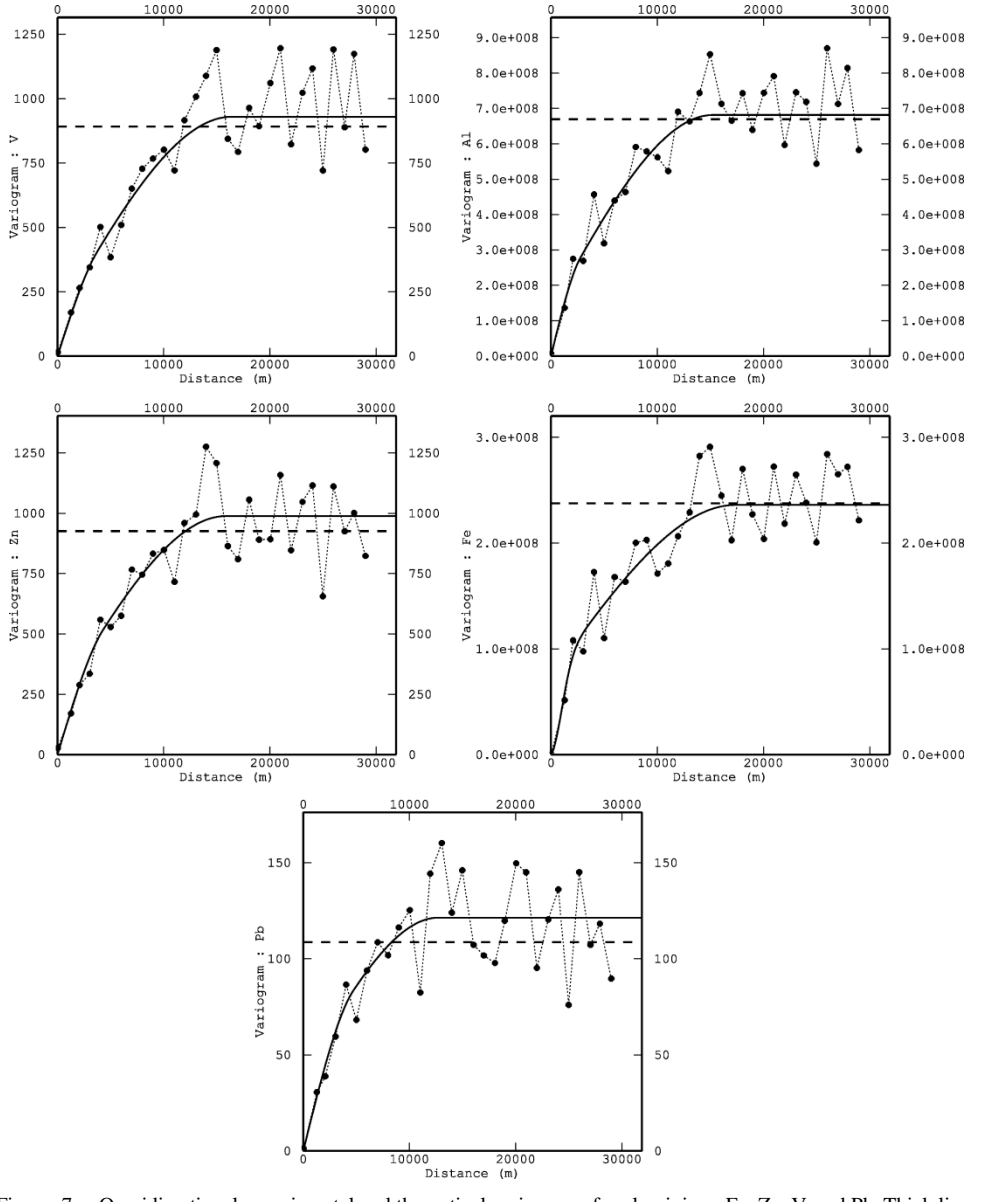

Figure 7. Omnidirectional experimental and theoretical variograms for aluminium, Fe, Zn, V, and Pb. Thick lines are for the modelled theoretical variograms, thin dashed lines are for the experimental variogram, and thick dashed lines are for the samples' variance. The two nested components at 2.5–4.7 and 12.7–17.4 km, respectively, are evident.

the availability of pairs is unbalanced in such a direction. The variogram map suggests that the maximum amount of lags be reduced to 30 (30 km with 1 km lags), in order to keep the same pairs availability both in long-shore and in cross-shore directions [65]. From now on, our estimations will be based on a variogram implemented with a lag value of 1 km and a total amount of 30 lags. Looking at such stationary modelled variograms (figure 7), we can note how, for aluminium, Fe, V, Zn, and Pb, two distinct components of spatial variability are clearly evident. These two different trends act at different spatial scales, one shorter with a higher frequency variability and one larger with a smoother field variation. Importantly, we

are assuming the variables are a linear combination of two distinct effects and a constant local mean. Short-range variability acts on a spatial scale of about 2.5–4.7 km, while long-range variability acts on a spatial scale of about 12.7–17.4 km. There is no variability-scale structure smaller than the local one and none bigger than the regional one, and both are similarly centred on a regional mean value. To verify the assumption of the nested structure in the experimental variogram, we attempted to use only one function (figure 8). In the example, the aluminium variogram is not correctly fitted by a spherical or exponential model. In fact, the first is unable to capture the first lag behaviour correctly (figure 8a), and the second (figure 8b) does not fit the highest lags (the sill) properly. A nested variogram with two range models is thus considered more appropriate.

The experimental variogram of Hg shows a completely unstructured spatial variability, with a pure nugget effect through the entire spatial domain (figure 9a). As discussed before, Hg shows a highly skewed distribution that seems to be reflected in the variogram computation results. By transforming the variable in its natural logarithm, the experimental variogram becomes much more reasonable (figure 9b), with one spherical structure and a range of 7.7 km. Arsenic, Cr, Cu, and Ni show only one well-designed structure (a spherical one) with a unique range, varying from 14 to 20 km, and a nugget effect, more evident for arsenic (figure 10).

Cadmium, whose variogram is extremely confused, when filtered by the unique outlier, assumes a more conventional shape. Details of all the modelled theoretical variograms are listed in table 4.

4.3 *Spatial estimations*

Once the structural analysis has been implemented, estimation processes can be applied for correct modelling of the variability structure for the different heavy metals. Kriging of spatial components here is computed to identify the two different spatial factors explaining the spatial distribution of the variables.

In many cases, the spatial distribution of a variable is the result of an extremely complex mixture of different factors, often acting at different temporal or spatial scales. Variogram is a powerful tool to extract such a multi-scale configuration and, coupled with the kriging estimation method, can be used to identify each spatial component. If the variable can be regarded as $Z(x) = \sum_{u=0}^{S-1} Z_u(x)$, where $Z_u(x)$ denotes the independent variables that amount to $Z(x)$, its variogram will be $\gamma(h) = \sum_{u=0}^{S-1} \gamma_u(h)$, where $\gamma_u(h)$ denotes the spatial components of the global variogram $\gamma(h)$. Now, we can implement ordinary punctual kriging, introducing into the kriging system only one spatial component at once and computing the estimation for

Table 4. Theoretical variograms parameters in details.

Variable	Model
Al	1.29e008 * sph(2.79e003) + 5.52e008 * sph(15.23e003)
Fe	7.40e007 * gaus(2.49e003) + 1.62e008 * sph(17.37e003)
Cr	30.52 + 547.78 * sph(15.67e003)
Cu	14.38 + 132.21 * sph(14.46e003)
Ni	8.55 + 151.63 * sph(16.05e003)
V	140.66 * sph(3.76e003) + 788.98 * sph(16.40e003)
Zn	208.60 * sph(4.33e003) + 779.56 * sph(15.86e003)
Pb	40.42 * sph(4.72e003) + 80.95 * sph(12.68e003)
Cd	0.014 * sph(2.13e003)
As	30.90 + 47.61 * sph(20.00e003)

Note: *sph* and *exp* denote spherical and exponential models, respectively.

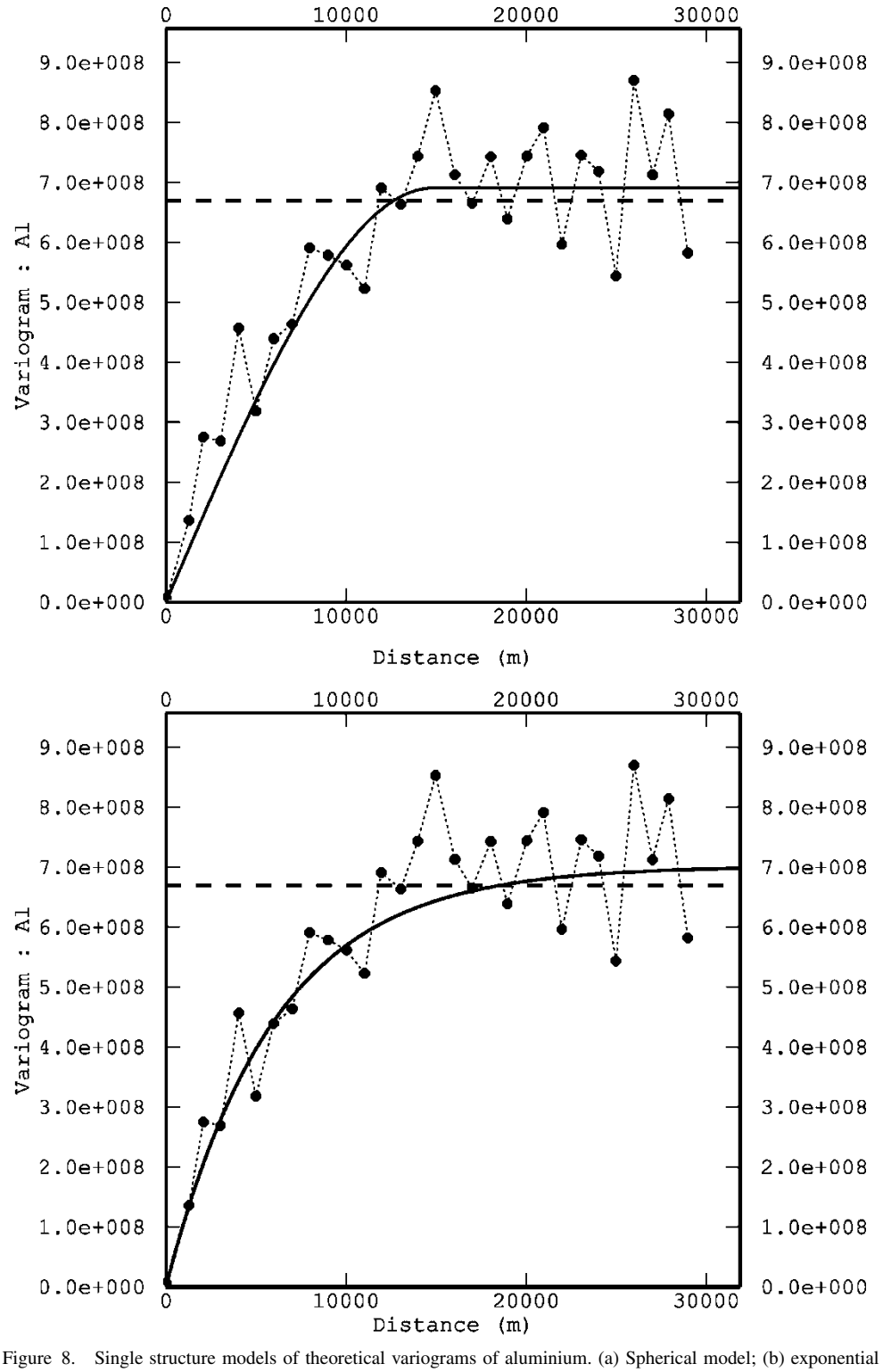

Figure 8. Single structure models of theoretical variograms of aluminium. (a) Spherical model; (b) exponential model. The ranges are 14.800 and 17.950 km, respectively.

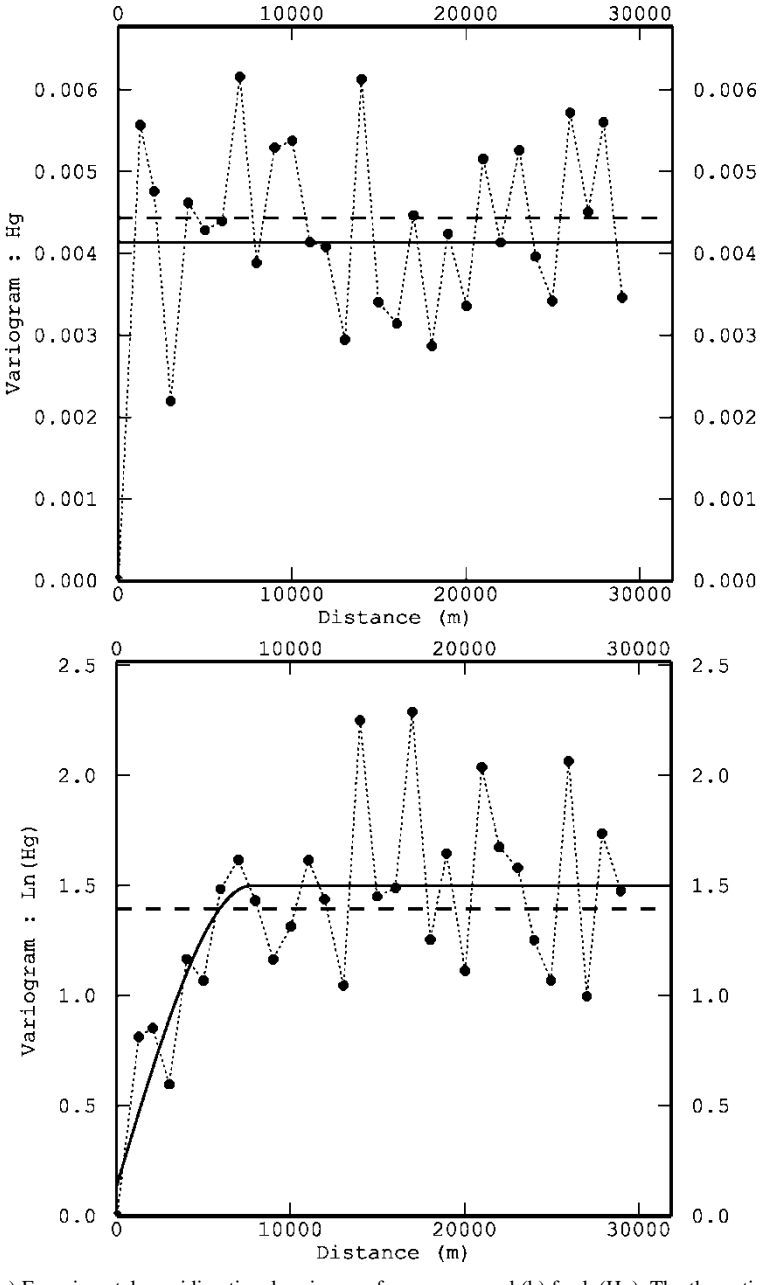

Figure 9. (a) Experimental omnidirectional variogram for mercury and (b) for ln(Hg). The theoretical variogram of transformed variable is: $\gamma(h) = 0.13 + 1.36\ sph(7.76e003)$.

each component. The linear combination will be $\tilde{Z}(x_0) = \sum_{a=1}^{n} \lambda_a^u Z(x_a)$, where the apex u denotes the u_{th} spatial component, while the kriging system will be:

$$\begin{cases} \sum_{b=1}^{n} \lambda_b^u \gamma_{a,b} - \mu^u = \gamma_{a,0}^u \\ \sum_{a=1}^{n} \lambda_a^u = 1, \end{cases}$$

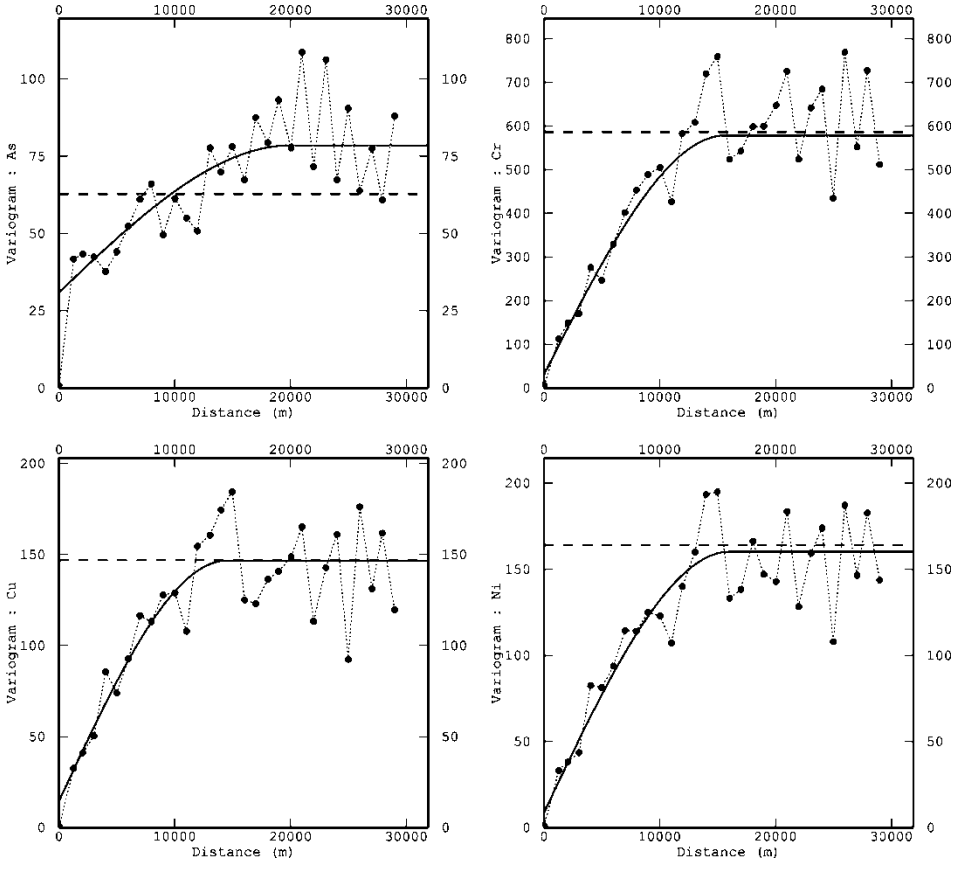

Figure 10. Experimental omnidirectional variograms for As, Cu, Cr, and Ni, showing the only one component structured variability. See figure 7 caption for details.

where γ^u represents the u_{th} model component. With such a procedure, it is possible to extract the different spatial distributions of all the independent variables that sum up the original one.

In our case, the components sum up to two, and we can consider the variable as a combination of a local/high-frequency component and a regional/low-frequency component and their estimation as a filtering algorithm that allows us to distinguish one component from another. We are assuming that both components are second-order stationary, according to the aforementioned quasi-stationarity assertion.

Looking at the kriged map of the regional range (figure 11a) component of zinc (reported as an example for the other nested variability structures), we can easily see a smoothed variation of the field, with low-frequency variability through the entire spatial domain. An essentially grain-size-driven distribution of values can be assumed, with generally high concentration levels corresponding to the finest sediment, distributed outside the shelf zone and in the Golfo di Policastro zone and low-concentration values generally concentrated along the coast and out of the Punta Licosa area, where a coarser sediment is more diffuse. The local range component grid (figure 11b) shows a high-frequency variability with several high- and low-concentration hot-spot values. Mainly, from Punta Licosa to Camerota Cape, the anomalies are more apparent, while a negative spot is located in the middle of Golfo di Policastro.

Finally, the map (figure 11c) obtained by traditional implementation of ordinary punctual kriging [49] on the global nested variogram shows both short- and long-range components

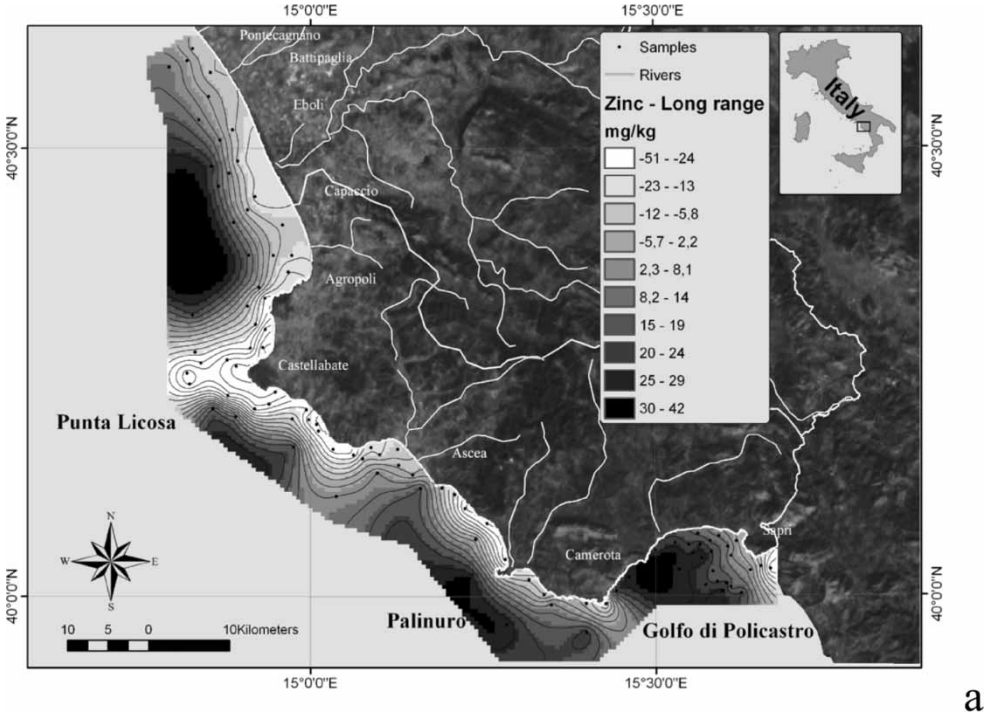

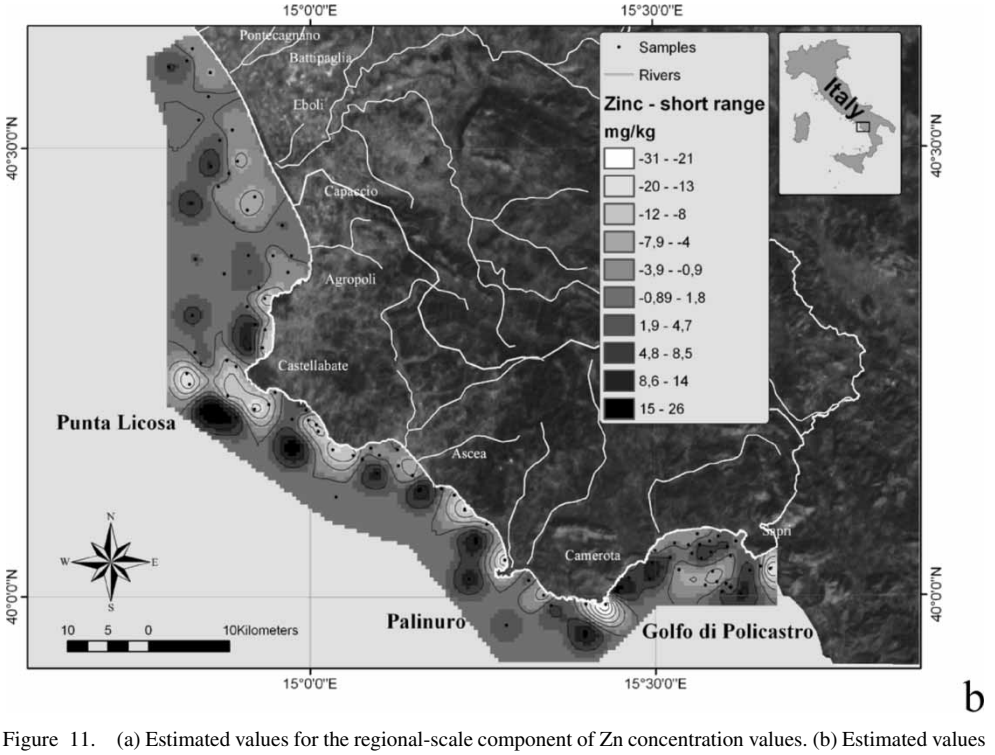

Figure 11. (a) Estimated values for the regional-scale component of Zn concentration values. (b) Estimated values for the local-scale component of Zn concentration values. (c) Ordinary punctual kriging map of the combined regional and local structures of variability of Zn. For both (a) and (b), the mean constant value of 72.66 mg kg^{-1} is subtracted. The resolution of the interpolated map is 500 m.

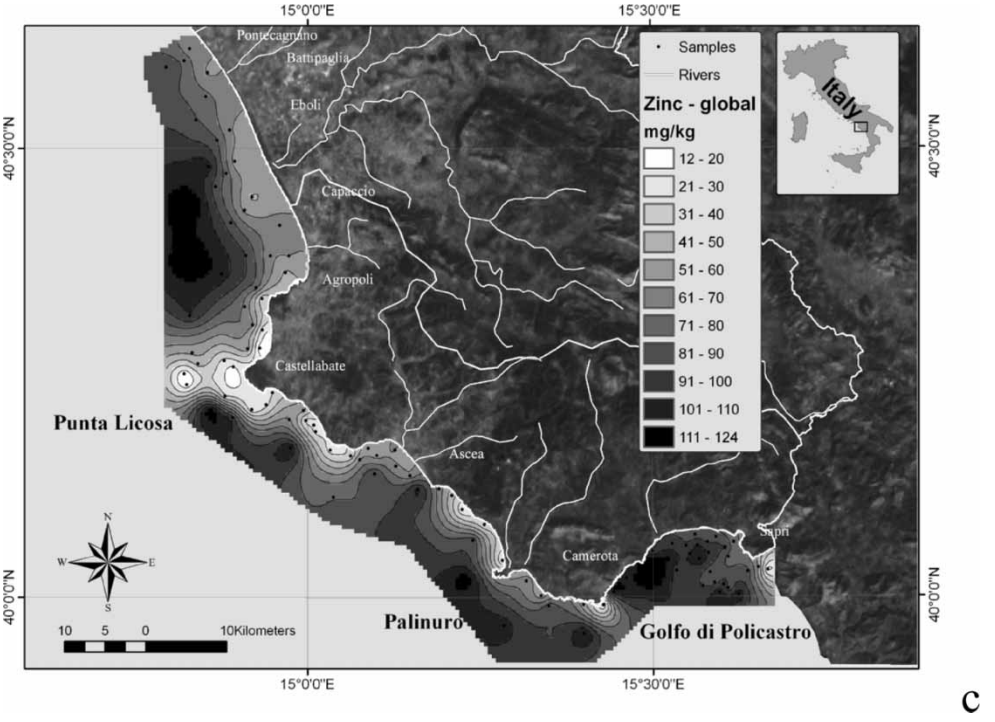

Figure 11. Continued.

and represents the complete description of the general distribution of estimated concentration values for the different trace metals.

Box-Whiskers plots (figure 12) of the distribution parameters of spatial components of the studied trace metals show several particular features; the median value is substantially constant for both components, while the measure of dispersion (interquartile range) is very different. In fact, heavy metals characterized by a nested variability structure can be considered as the sum of a mean value (a spatial mean, constant for the whole spatial domain, accordingly with the second-order stationarity principle) and two spatial components that act at two different spatial scales. This is why the median value is reasonably constant for both components. Regional-scale dispersion is much higher than that of the local scale just because of the different sill values (the variance modelled by the variogram). The sill of the regional component is much higher than the local one, and the dispersion of estimated data is greater.

The regional-scale component is a somewhat globally variable surface in which the more irregular high-frequency variations of the local-scale component is filtered out. Thus, these median values for the regional components can be reasonably regarded as the background levels of the different heavy metals (figure 13). Median values of the estimated regional scale components can be higher (or lower) than the raw data, filtering local anomalies related to localized sources or high-frequency grain-size distribution patterns. Obviously, for the heavy metals that do not present nested structures in the study area, the estimated background value are simply the median of the global kriged map.

To summarize, median values of 48238, 36448, 75.23, 80.39, and 21.43 mg kg^{-1} were calculated for aluminium, Fe, V, Zn, and Pb, respectively. For the heavy metals characterized by non-nested variograms (Cr, Cu, Ni, and As), median values are 51.05, 24.57, 28.91, and 21.49 mg kg^{-1}, respectively. Cadmium, whose variogram has been calculated on the filtered

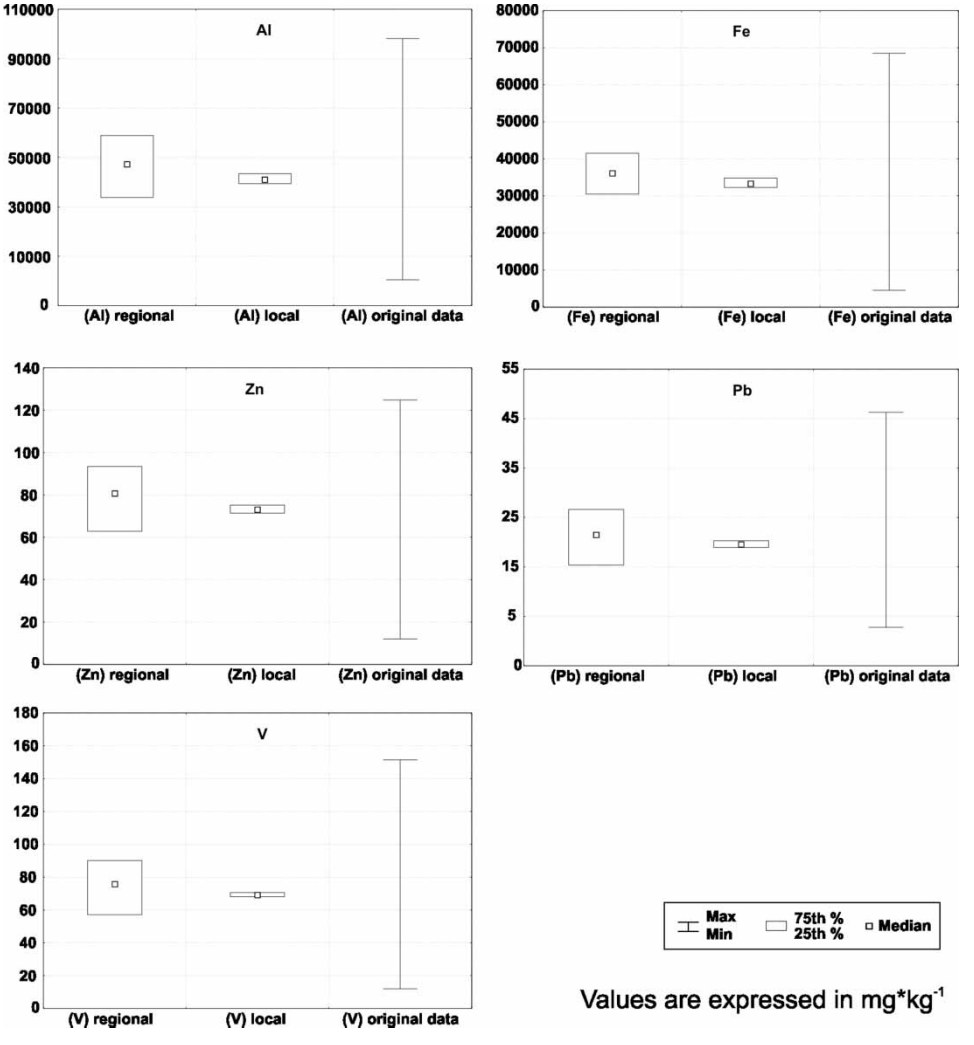

Figure 12. Box-Whiskers plots of the distribution parameters (median and I and II quartiles) of spatial components for aluminium, Fe, Zn, Pb, and V. The interval bar refers to the range of variability of the original concentration values of the same analytics.

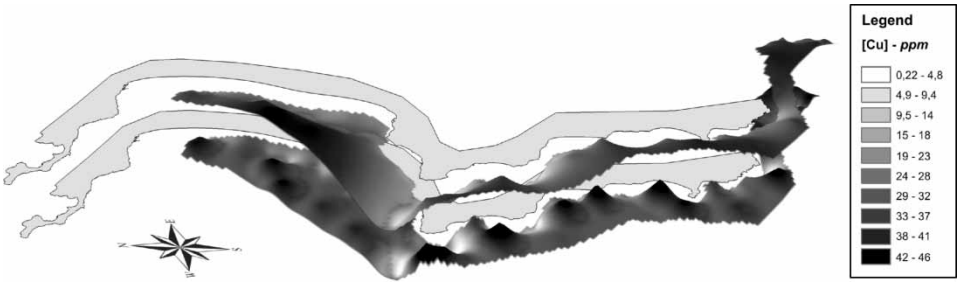

Figure 13. Three-dimensional representation of regional (up) and local (bottom) variability components of zinc.

dataset, shows a background value of 0.16 mg kg^{-1}, while Hg, for which log-normal kriging was implemented, shows an estimated background value of 0.07 mg kg^{-1}.

5. Conclusions

(1) Stationary and non-stationary geostatistical analyses carried out on a multidimensional dataset of heavy metals, grain size, and organic carbon contents were used to define a 2D spatial scale conceptual model and an appropriate assessment of marine geochemical baselines of trace elements characterized by multi-range spatial distribution patterns.
(2) Geochemical backgrounds for the southern Campania shelf area were calculated for Al, Fe, Cd, V, Cr, Zn, Cu, Ni, As, Hg, and Pb. Primary control of grain size on the distribution patterns of most of the studied heavy metals is evident at both local and regional spatial scales. Arsenic shows a particular behaviour with high concentrations related to an important hydrothermal activity typical of the southern Campania area.
(3) The limited contribution from anthropogenic pollution to the environment being studied is testified by the estimated enrichment factors (generally $\sim$1 for most trace elements) that rather suggest a direct control for the facing continental area on the concentration values of the heavy metals considered in the marine sediments.

Acknowledgements

We thank Patricia Sclafani, who revised the English text. Mauro Frignani is thanked for helpful discussions and careful reading of a preliminary version of the manuscript. Financial support was provided by the *GEOMARE Sud* Institute of CNR, Naples, Italy.

References

[1] R.J. Horwarth, I. Thornton. Regional geochemical mapping and its application to environment studies. In *Applied Environmental Geochemistry*, I. Thornthon (Ed.), pp. 41–73, Academic Press, London (1983).
[2] B. Bolviken, J. Bergströ, A. Bjorklund, M. Kontio, P. Lehmuspelto, T. Lindholm, J. Magnusson, R.T. Ottesen, A. Steenfelt, T. Volden. *Geochemical Atlas of Northern Fennoscandia. Scale 1:400,000*. Geological Surveys of Finland, Norway and Sweden (1986).
[3] A.G. Darnley. International geochemical mapping and the environment. *J. Geochem. Explor*., **41**, 81–83 (1991).
[4] British Geological Survey. *Regional Geochemical Atlas Series. Great. Glen*, British Geological Survey, Keyworth, UK (1987).
[5] British Geological Survey. *British Geological Survey. Regional Geochemical Atlas Series. Argyll*, British Geological Survey, Keyworth, UK (1990).
[6] British Geological Survey. *Regional Geochemical Atlas Series. East Grampians*, British Geological Survey, Keyworth, UK (1991).
[7] British Geological Survey. *Regional Geochemical Atlas Series. Lake District*, British Geological Survey, Keyworth, UK (1992).
[8] British Geological Survey. *North East England, Regional Geochemical Atlas Series*. Keyworth, UK (1997).
[9] A.G. Darnley. International geochemical mapping: a new global project. *J. Geochem. Explor*., **39**, 1–13 (1990).
[10] A.G. Darnley, A. Bjorklund, B. Bolkiven, N. Gustavsson, P.V. Koval, J.A. Plant, A. Steenfelt, M. Tauchid, X. Xie. A global geochemical database for environmantal and resource management. Recommendation for international geochemical mapping. *Final Report of IGCP Project 259, Earth Sciences 19*, UNESCO, Paris (1995).
[11] S. Covelli, G. Fontolan. Baseline Geochemical mapping of Sardinia. *J. Geochem. Explor.*, **60**, 77–90 (1997).
[12] B. De Vivo, M. Boni, A. Marcello, M. Di Bonito, A. Russo. Baseline geochemical mapping of Sardinia (Italy). *J. Geochem. Explor*., **60**, 77–90 (1997).
[13] R. Salminen, T. Tarvainen. The problem of defining geochemical baselines. A case study of selected elements and geological materials in Finland. *J. Geochem. Explor*., **60**, 91–98 (1997).
[14] C. Ferguson, D. Darmendrail, K. Frier, B.K. Jensen, J. Jensen, H. Kasamas, A. Urzelai, J. Vegter. *Risk Assessment for Contaminated Sites in Europe*, *Vol. 1, Scientific Basis*, LQM Press, Nottingham, UK (2005).
[15] B. De Vivo, M. Boni, S. Costabile. Formational anomalies versus minimum pollution, geochemical risk maps of Sardinia, Italy. *J. Geochem. Explor*., **64**, 321–337 (1998a).

[16] B. De Vivo, F. Riccobono, G. Esabatini (Eds.). *Cartografia Geochimica Ambientale. Primi Esempi di Applicazione: Calabria, Peloritani, Sardegna e Toscana Meridionale*. Monografia memorie descrittive della carta geologica d'Italia. Servizio Geologico Nazionale, LV (1998b).
[17] R. Salminen, T. Tarvainen, A. Demetriades, M. Duris, F.M. Fordyce, V. Gregorauskiene, H. Kahelin, J. Kivisilla, G. Klaver, H. Klein, J.O. Larson, J. Lis, J. Locutura, K. Marsina, H. Mjartanova, C. Mouvet, P. O'Connor, L. Odor, G. Ottonello, T. Paukola, J.A. Plant, C. Reimann, O. Schermann, U. Siewers, A. Steenfelt, J. Van Der Sluys, B. De Vivo, L. Williams. *Foregs Geochemical Mapping Field Manual. Guide 47, Geological Survey of Finland*, Espoo (1998).
[18] D. Bodis, S. Rapant. *Geochemical Atlas of The Slovak Republic*. Ministry of Environment of Slovak Republic, Geological Survey of Slovak Republic (1999).
[19] A.G. Darnley. Global geochemical mapping and its implementation in the Asia-Pacific region. *Appl. Geochem.*, **16**, 1309–1321 (2001).
[20] B. De Vivo, G. Rolandi (Eds). Mount Vesuvius and volcanism of the Campanian plain. *Mineral. Petrol.*, **73**, 233 pp. (2001).
[21] M. Singh, G. Müller, I.B. Singh. Geogenic distribution and baseline concentration of heavy metals in sediments of the Ganges River, India. *J. Geochem. Explor*., **80**, 1–17 (2003).
[22] A.J. Sinclair. Estimation of the geochemical threshold and its statistical significance. *J. Geochem. Explor*., **3**, 129–149 (1974).
[23] A.J. Sinclair. *Application of Probability Graphs in Mineral Exploration. Special Volume 4*, Association of Exploration Geochemists, Rexdale, Ont., Canada (1976).
[24] A.W. Rose, J.E. Hawkes, J.S. Webb. *Geochemistry in Mineral Exploration*, 2nd ed., Academic Press, London (1979).
[25] A.J. Sinclair. A fundamental approach to threshold estimation in exploration geochemistry. Probability plots revisited. *J. Geochem. Explor*., **41**, 1–22 (1991).
[26] Q. Cheng, F.P. Agteberg, S.B. Ballantyne. The separation of geochemical anomalies from background by fractal method. *J. Geochem. Explor*., **51**, 109–130 (1994).
[27] Q. Cheng. Multifractal modeling and spatial analysis with GIS: Gold potential estimation in the Mitchell-Sulphurets area. Northwestern British Columbia. Unpublished PhD thesis. University of Ottawa, Ottawa (1994).
[28] Q. Cheng, F.P. Agtemberg, G.F. Bonham-Carter. A spatial analysis method for geochemical anomaly separation. *J. Geochem. Explor*., **56**, 183–195 (1996).
[29] Q. Cheng, Y. Xu, E. Grunsky. Integrated spatial and spectrum analysis for geochemical anomaly separation. In *Proceedings of the International Association for Mathematical Geology Meeting*, Trondheim, Norway, S.J. Lippard, A. Naess, R. Sinding-Larsen (Eds), **1**, 87–92 (1999).
[30] Q. Cheng, Y. Xu, E. Grunsky. Integrated spatial and spectrum method for geochemical anomaly separation. *Nat. Resour. Res*., **9**, 43–56 (2000).
[31] Q. Cheng, G.F. Bonham-Carter, G.L. Raines. GeoDAS: A new GIS system for spatial analysis of geochemical data sets for mineral exploration and environmental assessment. In *20th International Geochemical Exploration Symposium (IGES)*, Santiago de Chile, 6/5–10/5, 42–43 (2001).
[32] J. Plant, D. Smith, B. Smith, L. Williams, M. Karger, S. Sandomirsky. Multidimensional statistical technique for detection of low constrast geochemical anomalies. *J. Geochem. Explor*., **72**, 47–58 (2001).
[33] A.P. Reis, A.J. Sousa, E. Ferreira da Silva, C. Patina, E.C. Fonseca. Combining multiple correspondence analysis with factorial kriging analysis for geochemical mapping of the gold-silver deposit at Marrancos (Portugal). *Appl. Geochem*., **19**, 623–631 (2004).
[34] F. Ortolani, M. Torre. Guida all'escursione dell'area interessata dal terremoto del 23.11.1980. *Rendiconti Società Geologica Italiana*, **4**, 173–214 (1981).
[35] F. Ghisetti, L. Vezzani. Contribution of structural analysis to understanding the geodynamic evolution of the Calabrian Arc (Southern Italy). *J. Struct. Geol*., **3**, 371–381 (1981).
[36] K. Kastens, J. Mascle, C. Auroux, E. Bonatti, C. Broglia, J. Channel, P. Curzi, K. Emeis, G. Glacon, S. Hasegawa, W. Hieke, R. Mascle, R. Sartori, R. Sprovieri, M. Torii. ODP Leg 107 in the Tyrrhenian Sea: Insights into passive margin and back-arc basin evolution. *Geol. Soc. Am. Bull*., **100**, 1140–1156 (1988).
[37] L. Brancaccio, A. Cinque, G. Belluomini, M. Branca, L. Delitalia. Isoleucine epimerization dating and tectonic significance of upper Pleistocene sea-level feature of the Sele Plain (Southern Italy). *Z. Geomorphol. N.F*. Suppl., **62**, 159–166 (1986).
[38] F. Russo. I sedimenti quaternari della Piana del Sele, studio geologico e geomorfologico. PhD thesis, University Federico II, Naples (1990).
[39] F. Ippolito, F. Ortolani, M. Russo. Struttura marginale tirrenica dell'Appennino campano: reinterpretazione di dati di antiche ricerche di idrocarburi. *Memorie Società Geologica Italiana*, **12**, 227–250 (1973).
[40] AGIP. *Temperature Sotterranee. Inventario dei dati Raccolti dall'Agip Durante la Ricerca e la Produzione di Idrocarburi in Italia*, Agip, Milan (1977).
[41] R. Bartole, C. Savelli, M. Tramontana, F.C. Wezel. Structural and sedimentary features in the Tyrrhenian margin off Campania, Southern Italy. *Mar. Geol*., **55**, 163–180 (1984).
[42] F. Trincardi, M.E. Field. Geometry, lateral variation and preservation of downlapping regressive shelf deposits: eastern Tyrrhenian Sea Margin, Italy. *J. Sediment. Petrol*., **61**, 775–790 (1991).
[43] L. Ferraro, T. Pescatore, B. Russo, M.R. Senatore, C. Secchione, M.G. Coppa, A. Di Tuoro. Studi di geologia marine del margine tirrenico: la piattaforma continentale tra Punta Licosa e Capo Palinuro (Tirreno Meridionale). *Boll. Soc. Geol. Ital*., **116**, 473–485 (1997).

[44] A. Argnani, G. Bortoluzzi, A. Bozzani, A. Canepa, M. Ligi, V. Palombo, P. Serracca, F. Trincardi. Sedimentary dynamics on the Eastern Tyrrhenian Margin: preliminary report. *G. Geol*., **51**, 165–178 (1989).
[45] C.K. Wentworth. A scale of grade and class terms for clastic sediments. *J. Geol*., **30**, 377–392 (1922).
[46] L.G. Schultz. *Quantitative Interpretation of Mineralogic Composition from X-Ray and Chemical Data for the Pierre Shale*. US Geological Survey, Professional Paper (1964).
[47] E. Barahona, F. Huertas, A. Pozzuoli, J. Linares. Mineralogia e genesi dei sedimenti della provincia di Granata (Spagna). *Mineral. Petrogr. Acta*, **26**, 61–90 (1982).
[48] P. Pohl. Hydride generation – recent advances in atomic emission spectrometry. *Tr. Anal. Chem*., **23**, 87–101 (2004).
[49] M. Armstrong. *Basic Linear Geostatistics*, Springer, Berlin (1998).
[50] K.H. Wedepohl. *Handbook of Geochemistry*, Springer, Berlin (1978).
[51] B. De Vivo, A. Lima, S. Albanese, D. Cicchella. *Atlante di Geochimica-Ambientale della Regione Campania*, Di Frede (Ed.) (2003).
[52] J.M. Martin, M. Meybeck. Elemental mass-balance of material carried by major world rivers. *Mar. Chem*., **7**, 173–206 (1979).
[53] B. De Vivo, H.E. Belkin, M. Barbieri, W. Chelini, P. Lattanzi, A. Lima, L. Tolomeo. The Campi Flegrei (Italy) geothermal system: a fluid inclusion study of the Mofete and San Vito fields. *J. Volcanol. Geotherm. Res*., **36**, 303–326 (1989).
[54] B. De Vivo, M. Boni, A. Marcello, M. Di Bonito, A. Russo. Environmental geochemistry at global scale. *Appl. Geochem*., **16**, 1291–1308 (2001).
[55] C. Federico, A. Aiuppa, P. Allard, S. Bellomo, A. Michel, F. Parello, M. Valenza. Magmatic gas–water interactions at Vesuvius volcano: major, minor and trace element composition of the volcanic aquifer. *Geochim. Cosmochim. Acta*, **66**, 963–981 (2002).
[56] R.E. Stauffer, J.M. Thompson. Arsenic and antimony in geothermal waters of Yellowstone national park, Wyoming, USA. *Geochim. Cosmochim. Acta*, **48**, 2547–2561 (1984).
[57] S. Goldberg. Chemical modeling of arsenate adsorption on aluminium and iron oxide minerals. Soil. *Sci. Soc. Am. J.*, **50**, 1154–1157 (1986).
[58] C.A. Heinrich, P.E. Eadington. Thermodynamic predictions of the hydrothermal chemistry of arsenic, and their significance for the paragenic sequence of some cassirite–arsenopyrite-base metal sulphide deposits. *Econ. Geol*., **81**, 511–529 (1986).
[59] J.M. Ballantyne, J.N. Moore. Arsenic geochemistry in geothermal systems. *Geochim. Cosmochim. Acta*, **52**, 475–483 (1988).
[60] R.L. Stanton. *Ore Elements in Arc Lavas*, Clarendon Press, Oxford (1994).
[61] D.A. Nimick, J.N. Moore, C.E. Dalby, M.W. Savka. The fate of geothermal arsenic in the Madison and Missouri Northwestern British Columbia. Unpublished PhD thesis. University of Ottawa, Ottawa (1998).
[62] E.H. Isaaks, R.M. Srivastava. *An Introduction to Applied Geostatistics*, Oxford University Press, Oxford (1989).
[63] M. Rosenbaum, M. Soderstrom. Geostatistics as an aid to mapping (1996). Available online at: http://gis.esri.com/library/userconf/europroc96/PAPERS/PN11/PN11F.HTM, accessed 2005.
[64] H. Wackernagel. *Multivariate Geostatistics. An Introduction with Application*, Springer, Berlin (2003).
[65] P.A. Burrough, R.A. McDonnell. *Principles of Geographical Information Systems*, Oxford University Press, Oxford (1997).